GCAGS JOURNAL
A Publication of the Gulf Coast Association of Geological Societies
www.gcags.org

Depositional Systems, Lithofacies, and Reservoir Characterization of the Upper Cretaceous Austin Chalk, Brookeland and Burr Ferry Fields in East Texas and Western Louisiana

Robert G. Loucks, Sheng Peng, Kelly E. Hattori, Priyanka Periwal, Josh R. Lambert, Christopher K. Zahm, and Lucy T. Ko

Bureau of Economic Geology, Jackson School of Geosciences, University of Texas at Austin, Box X, University Station, Austin, Texas 78713–8924, U.S.A.

ABSTRACT

The Upper Cretaceous Austin Chalk reservoirs produce from argillaceous marly chalks and chalky marls along a broad play trend from the Texas-Mexico border into Louisiana. A series of cores from the Brookeland, Burr Ferry, Burr Ferry North, and Burr Ferry South field areas in East Texas and western Louisiana allow for the characterization of these argillaceous Austin Chalk reservoirs in those areas and the chance to develop a reservoir analog with associated reservoir-characterization concepts for other Austin Chalk fields. The chalks in the study area were deposited on a deeper-water shelf behind the relict Lower Cretaceous Stuart City Reef trend and on the upper-slope area in front of the paleo-reef margin. A variety of lithofacies were deposited in the Austin Chalk, where the two main groups are well-bioturbated, organic-matter-poor to -fair, marly chalks to chalky marls and well-laminated, organic-matter-rich, marly chalks to chalky marls. The stacking patterns of the interbedded lithofacies with variable argillaceous content and fabrics creates vertical heterogeneity relative to mechanical strength and other reservoir properties. The pore network is predominantly interparticle nano- and micropores between coccolith fragments; however, these nano- and micropores are segmented by clay-mineral platelets that reduce pore-throat sizes and thus permeability. Overall, reservoir quality is low with mean porosity at 5.8% and geometric mean permeability at 285 nd. Major observations include: (1) Austin Chalk argillaceous chalks produce from a range of lithofacies with variable reservoir properties; (2) reservoir quality is low with pore sizes mainly in the nanometer range; (3) source-rock quality in the laminated lithofacies is good and can contribute to self-sourcing; and (4) vertical heterogeneity can be high, while subregional lateral heterogeneity is low.

INTRODUCTION

The Upper Cretaceous Austin Chalk trend (Figs. 1A and 1B) has been an active exploration and development target in Texas and Louisiana since the 1920s (e.g., Dravis, 1981; Grabowski, 1984; Dawson et al., 1995). Many areas have been well studied along this subsurface trend with topics including general stratigraphy (e.g., Anderson, 1979; Ewing, 2013), resource assessment (e.g., Scholle, 1977; Pearson, 2012; Whidden et al., 2018), hydrocarbon source-rock potential (e.g., Grabowski, 1984; Hunt and McNichol, 1984; Dawson et al., 1995; Berg and Gangi, 1999), and fractures (e.g., Corbett et al., 1987; Wiltschko et al., 1991; Rijken and Cooke, 2001; Ferrill et al., 2017). A number of outcrop studies (e.g., Dravis, 1981; Lock, 1984; Loucks et al., 2013; Ferrill et al., 2017; Griffith et al., 2019; Cooper et al., 2020) have also been completed, but these areas are updip from the productive trend and are not generally applicable to the producing section downdip. Only recently have several studies been published on the detailed depositional systems, lithofacies, and reservoir characterization of the regional Austin Chalk producing trend (Loucks et al., 2020a, 2020b, 2021a, 2021b; Loucks and Peng, 2021; Loucks and Reed, 2022).

This present area of investigation in East Texas and westernmost Louisiana contains four large Austin Chalk fields: Brookeland, Burr Ferry, Burr Ferry North, and Burr Ferry South (Fig. 1C). Discoveries of these fields began in the 1990s (e.g., Hooks and Hubbard,1994; Petzet, 1995). Even though these fields have significant production from the Austin Chalk, very

Manuscript received April 25, 2022; revised manuscript received June 4, 2022; manuscript accepted June 5, 2022.

GCAGS Journal, v. 11 (2022), p. 37–57.

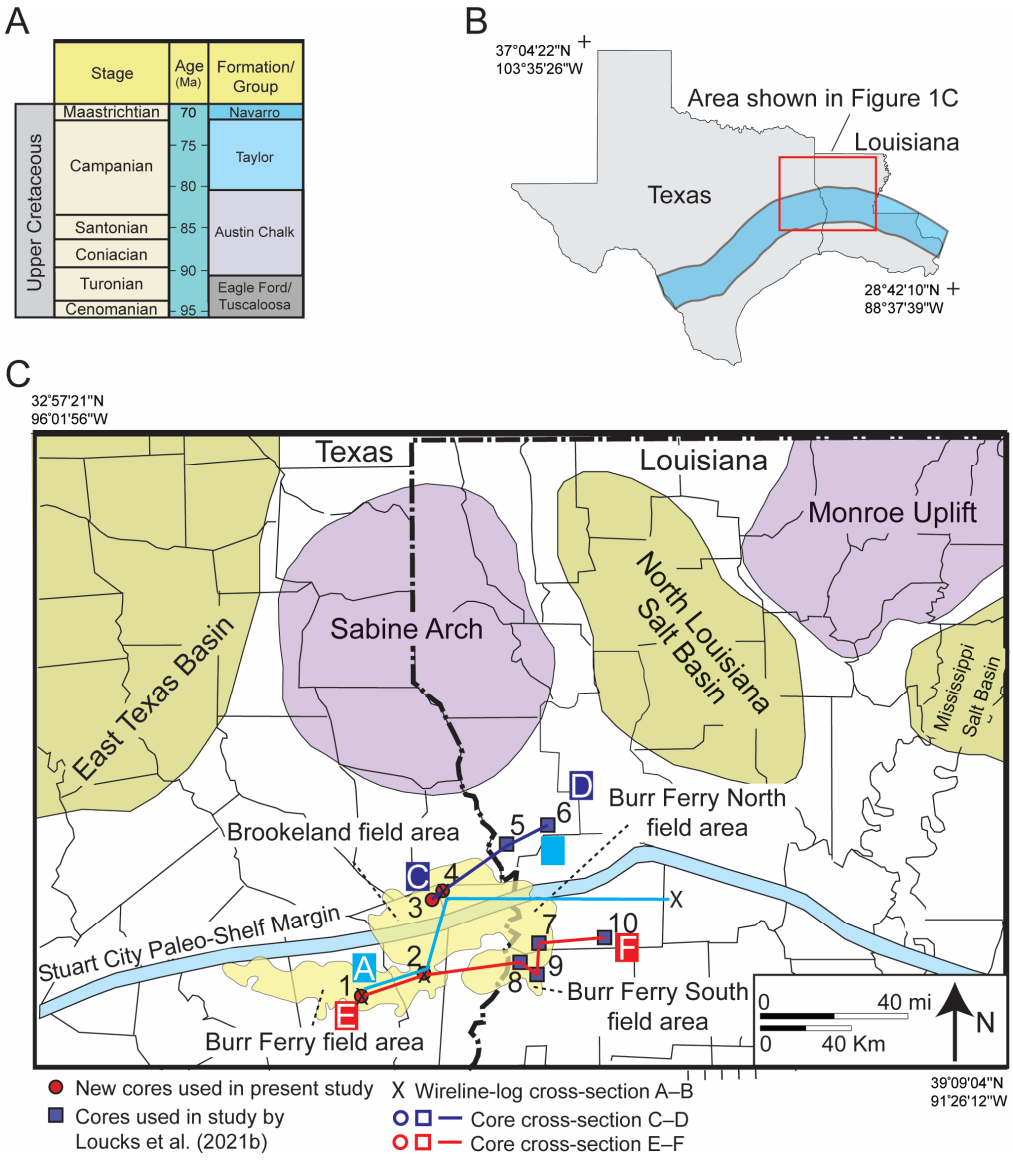

Figure 1. Age and location data for area of investigation. (A) Stratigraphic section for study area. Ages are from Walker et al. (2013). (B) Regional map showing the onshore Austin Chalk trend. Detailed area of investigation is shown by red box. (C) Map of study area showing major paleogeographic features and outlines of the Brookland, Burry Ferry, Burr Ferry North, and Burr Ferry South fields. Wireline-log locations used in wireline-log cross-section A–B in Figure 2 are plotted. Core locations and core-based stratigraphic sections C–D and E–F shown in Figure 3 are plotted. See Table 1 for identification details about the cores.

little is published about the geology or the associated reservoir characteristics in the area. However, a study by Loucks et al. (2021b) did describe some of the geology of the Burr Ferry North and Burr Ferry South fields in Louisiana. Some of the data and conclusions from that publication are incorporated into the present investigation, where appropriate, to allow for a more comprehensive geologic characterization of these Austin Chalk fields with perspective gained from the greater subregional scale of the present study.

The Austin Chalk is not a simple stratigraphic unit composed of homogeneous chalk, but rather is composed of a variety of argillaceous chalks (Loucks et al., 2020b, 2021b). Most of the Austin Chalk stratigraphic section throughout the trend displays strong vertical lithofacies changes with measurable differences in mineral composition, total organic carbon (TOC), mechanical strength, and reservoir quality. Therefore, the two major goals of this investigation are to define the geology of the Austin Chalk section from cores in the Brookeland, Burr Ferry, Burr Ferry North, and Burr Ferry South fields, and to develop concepts relative to argillaceous chalk reservoirs from these fields that can be applied elsewhere. Specific objectives are to (1) define the Austin Chalk depositional setting and environments in the Sabine Arch; (2) describe the range of lithofacies encountered; (3) present pore-type, porosity, and permeability analyses from cores in the area; (4) characterize type and abundance of organic matter; (5) provide some insights on micropetrography and mechanical stratigraphy; and (6) develop reservoir characterization principles from these fields that will aid in understanding the architecture and production of other argillaceous chalk reservoirs globally.

The data presented and concepts developed in this investigation can be used at the local scale to understand the stratal architecture in the producing fields and aid in the selection of optimal zones to land horizontal wells. On a regional basis, accomplishing the proposed objectives will aid in understanding the onshore Gulf of Mexico Austin Chalk trend and the concepts developed can be applied to production and development practices. Also, an in-depth, subregional investigation of argillaceous chalk reservoirs will advance the understanding of argillaceous chalk lithofacies control on pore types, pore networks, porosity, permeability, organic-matter types and abundance, and other reservoir characteristics.

DATA AND METHODS

This investigation of the subregional-scale characteristics of the Austin Chalk utilizes wireline logs and cores recovered from four wells in East Texas and six wells in far-western Louisiana (Table 1; Figs. 1C, 2, and 3). The cores in East Texas are newly described cores, whereas the Louisiana cores have been previously described in a study of the Austin Chalk completed by Loucks et al. (2021b). These two core datasets are integrated to extend the overall area of investigation to a subregional scale, while also increasing confidence in the validity of observed geological trends laterally and vertically throughout the formation.

Paleogeographically, four of the cores (cores 3–6) are located on the drowned shelf (i.e., onshelf), north of the relict (i.e., buried at time of Austin Chalk deposition) Lower Cretaceous Stuart City Reef trend; the other six cores (cores 1, 2, and 7–10) are on the upper-slope area, south of the relict reef trend (Fig. 1C). It is important to note that much of the differential topography between shelf and upper slope that existed at the time of the Stuart City Reef deposition (Lower Cretaceous) had been filled in by the time of Austin Chalk deposition, as shown by the limited seismic data reviewed by the present study. Core length ranges between 25 to 193 ft (7.6 to 58.8 m) (Fig. 3). The BP American No. 1 A–187 well cored 31 ft (9 m) of the Eagle Ford Group below the contact with the Austin Chalk above (core 2). The contact with the Taylor Group at the top of the Austin Group was captured in the Stonegate No. 1 Donner well in Louisiana where 44 ft (13.4 m) of the Taylor Group was recovered (core 5). The cores were described with a binocular microscope and the description was aided by 165 thin sections viewed with a petrographic microscope equipped with an ultraviolet (UV) light source. The thin sections were impregnated with blue epoxy to emphasize macropores where present and with blue, fluorescent dye to emphasize nano- and micropores with the application of UV light.

Micropetrography (i.e., rock description at the nano- and micrometer scale) is necessary for describing extremely fine-grained rocks such as the Austin Chalk strata (Loucks et al., 2021a). For the present study, 25 ion-milled samples from Texas and Louisiana were imaged on a FEI Nova NanoSEM 430 field-emission scanning electron microscope (SEM) at the Bureau of Economic Geology. A moderate accelerating voltage of 10 to 15 kV and a working distance of 6 to 10 mm were used for imaging. Energy dispersive spectroscopy (EDS) analysis was conducted on all ion-milled samples to identify texture, fabric, and mineralogy of fine grains. Over 500 backscattered electron, secondary electron, and EDS images were collected and analyzed.

TOC and programmed pyrolysis data were analyzed on 49 samples from Texas throughout the study areas by the Bureau of Economic Geology using HAWK (Hydrocarbon Analyzer with Kinetics™) methodologies. Weatherford Laboratories analyzed 214 samples for TOC and pyrolysis parameters using Rock-Eval™ II on samples from Louisiana. These two datasets are integrated in this investigation. TOC versus S1 and S2 curves (from pyrolysis) are used to evaluate source-rock quality. Samples were ground using a mortar and pestle and sieved on 60 mesh (250 microns) to obtain a uniform grain size. Weighed aliquots (70 mg) were analyzed using a standard heating program (Espitalié et al., 1977; Lafargue et al., 1998) in which samples were heated nonisothermally from 180°C to 300°C (356°F to 572°F), held isothermally at 300°C (356°F) for 3 min, then heated at a rate of 25°C/min (45°F/min) up to 650°C (1202°F).

Semiquantitative X–ray diffraction (XRD) analysis for mineralogy was completed on 15 samples from an unnamed proprietary Texas core in this study by Core Lab in Houston, Texas. Additional XRD data (153 analyses) from four wells in western Louisiana that were analyzed by Weatherford Laboratory in Houston, Texas, and published in Loucks et al. (2020a, 2021b) are also included in the XRD–based ternary diagram in Figure 4. Both bulk and clay-mineral analyses were completed. Rock chips were disaggregated using a mortar and pestle and a slurry was prepared and spray-dried onto a mount to be analyzed.

Thirty-four (34) porosity and permeability analyses were run for reservoir-quality analyses using the modified gas expansion (MGE) method developed by Peng and Loucks (2016) and refined by Peng et al. (2019). The MGE analyses were run in the Unconventional Petrophysics Laboratory at the Bureau of Economic Geology. The samples are 1 in (2.54 cm) diameter core plugs. In this method, helium gas is introduced into a reference cell where the plug is in a core holder under a confining pressure of 2000 psi (13.8 MPa). Gas permeability was measured under equilibrium pore pressure of approximately 150 psi (1.03 MPa). The measurement was conducted at a temperature of 25±0.2°C (77±0.4°F). Matrix permeability is calculated on the basis of the late-phase pressure decay data. The reader is referred to Peng and Loucks (2016) and Peng et al. (2019) for more details on the experimental and analytical procedures.

A handheld microrebound hammer was used to characterize rock strength (unconfined compressive strength [UCS]) in three cores: O.I.L. Energy No. 1 McShane Trust core, ARCO No. C1 Musser Davis, and Union Pacific Resources B6 No. 1 Sonat Min-

Table 1. List of wells plotted on map in Figure 1C. Calculated vitrinite reflectance (R_o) values are listed. Cores in wells labeled 1 to 4 are newly described and cores in wells labeled 5 to 10 are from Loucks et al. (2021b).

Well #	Well name	API#	County/Parish	State	Calculated R_o
1	O.I.L. Energy No. 1 McShane Trust	42457303520000	Tyler	Texas	1.05%
2	ARCO No. 1 BP American A–187	42241307510000	Jasper	Texas	1.62%
3	ARCO No. 1 ARCO Fee A–246	42241305800000	Jasper	Texas	0.86%
4	Union Pacific Resources No. 1 ARCO Vastar Unit A–183	42351305160000	Newton	Texas	0.80%
5	Stonegate No. 1 Donner	17085220990000	Sabine	Louisiana	0.70%
6	Coffman No. 1 Cabra	17085207510000	Sabine	Louisiana	0.74%
7	Union Pacific Resources B6 No. 1 Sonat Minerals	17115201550000	Vernon	Louisiana	0.94% est.
8	ARCO No. 1 Singletary	17011206160000	Beauregard	Louisiana	0.89%
9	ARCO No. C1 Musser Davis	17011203250000	Beauregard	Louisiana	0.92%
10	Union Pacific Resources No. 17–1 Quinn	17115201570000	Vernon	Louisiana	1.00%

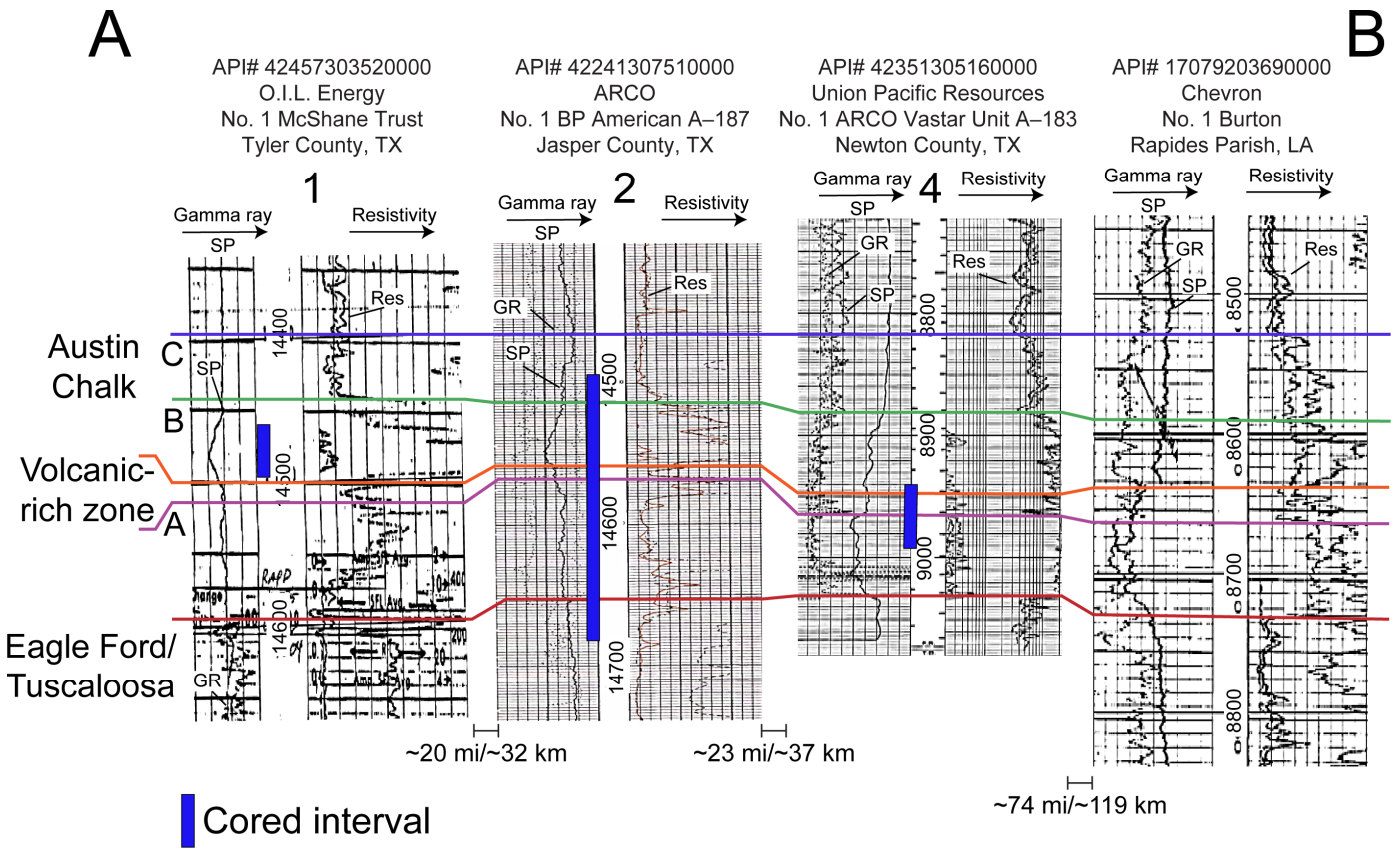

Figure 2. Wireline-log cross-section A–B composed of selected wireline logs in the area of investigation. Location of the cross-section is shown in Figure 1. The numbers above the first three wells are from the core location map. The fourth well on the right was not cored, but is a well-defined wireline log for picking tops. The thick, blue vertical line shows cored intervals.

erals. The method developed by Zahm and Enderlin (2010) and modified by Brooks et al. (2016) was followed. Sampling was done at a spacing of 2 to 4 in (5 to 10 cm), depending on the condition of individual core slabs.

STRATIGRAPHY AND GENERAL REGIONAL GEOLOGY

General Depositional Setting

The Austin Chalk marly chalk to chalky marl strata was deposited on a drowned, deeper-water platform below storm wave base as indicated by the dominance of open-marine, planktic biota such as coccolithophores, foraminifers, and calcispheres, as well as the presence of benthic inoceramid bivalves (Phelps et al., 2013; Loucks et al., 2021b). The nearest exposed continental land mass was the Appalachian (Ozarkian) land mass approximately 100 mi (160 km) north as shown by Blakey's (2011) paleogeographic map for this Late Cretaceous time period.

The study area straddles the relict shelf edge formed by the Lower Cretaceous Stuart City Reef trend (Fig. 1C). Present-day Austin Chalk burial depths on the drowned platform north of the shelf edge are shallower (7000 to 8500 ft [2100 to 2600 m]) than those south of the shelf edge on the upper slope (14,500 to 16,000 ft [4400 to 4900 m]). It is important to note that this exceptionally large difference in depth of burial is related to post-depositional, regional subsidence and tilting toward the Gulf of Mexico and does not represent original depositional relief. In fact, there may have been only several hundred feet (ca. 100 m) of relief across the shelf margin as pre-Austin Chalk sediment filled much of the original steep-rimmed architecture, smoothing the platform into a distally-steepened ramp.

Approximately 35 mi (55 km) north of the shelf edge is the southern boundary of the Sabine Arch (Fig. 1C), which separates the East Texas Basin and the North Louisiana Salt Basin. As shown by Loucks et al. (2021b), the uplifted Sabine Arch affected water depths between the arch and the shelf edge. Shallower-water (but still below storm wave base) lithofacies are dominant north of the shelf edge near the Sabine Arch, whereas the Austin Chalk is dominantly composed of deeper-water and anoxic-dominated lithofacies away from the Sabine Arch and south of the Stuart City paleo-shelf edge.

As recognized by Loucks et al. (2021a, 2021b), based on Blakey's (2011) paleogeographic map, the Florida and Yucatan peninsulas were drowned during Austin Chalk time and the ancient Gulf of Mexico was essentially an open-ocean setting. Reading and Collinson (1996) noted that present-day storm wave base is approximately 300 ft (90 m) off the open-marine east coast (i.e., Atlantic Ocean side) of Florida Peninsula. The depth to storm wave base during Austin Chalk time was probably similar or deeper. That would put Austin Chalk deposition in water depths of at least 300 ft (90 m) or more. The predominance of outer-shelf, open-marine, deep-water biota and the absence of surface-wave-produced hydrodynamic structures support this conclusion.

As noted by Loucks et al. (2021a, 2021b), based on lithofacies, trace elements, and TOC content, the bottom-setting conditions along the entire Austin Chalk trend varied between oxic, dysoxic, and anoxic conditions. These variations in depositional conditions are also reflected by the fabric of the strata ranging

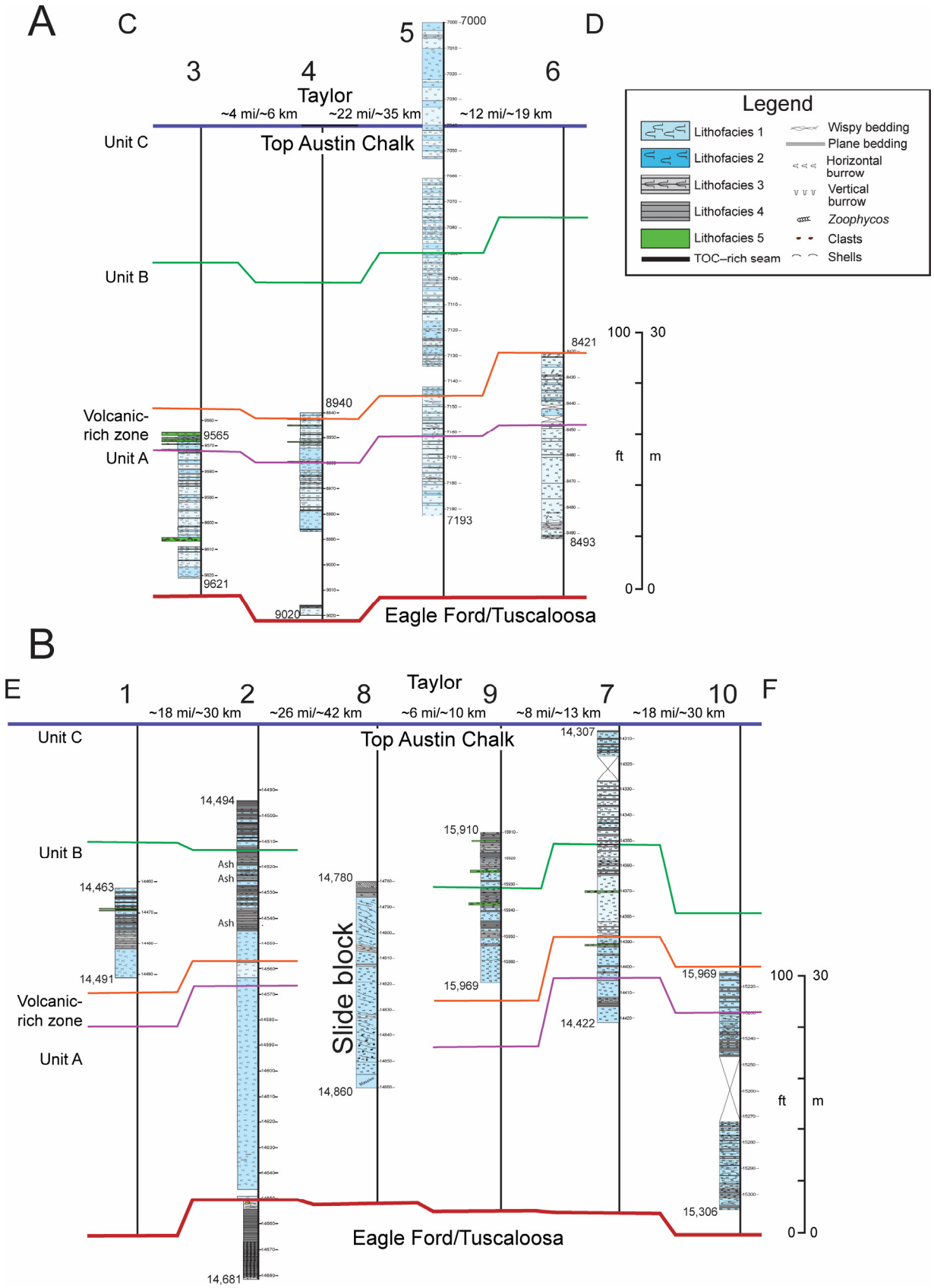

Figure 3. Stratigraphic core-based cross-sections. Note zone labeled "volcanic-rich zone." The basis for this zone is the strong positive gamma ray spikes and negative resistivity spikes. This zone is commonly labeled "volcanic-rich zone" on wire-line logs; see text for discussion. (A) Onshelf core cross-section C–D flattened on top of the Austin Chalk. Numbers refer to well names listed in Table 1. Line of section shown in Figure 1C. (B) Upper-slope core cross-section E–F flattened on top of the Austin Chalk. Numbers refer to well names listed in Table 1. Line of section shown in Figure 1C. Core 8 recovered a thick, slide block and is not correlated.

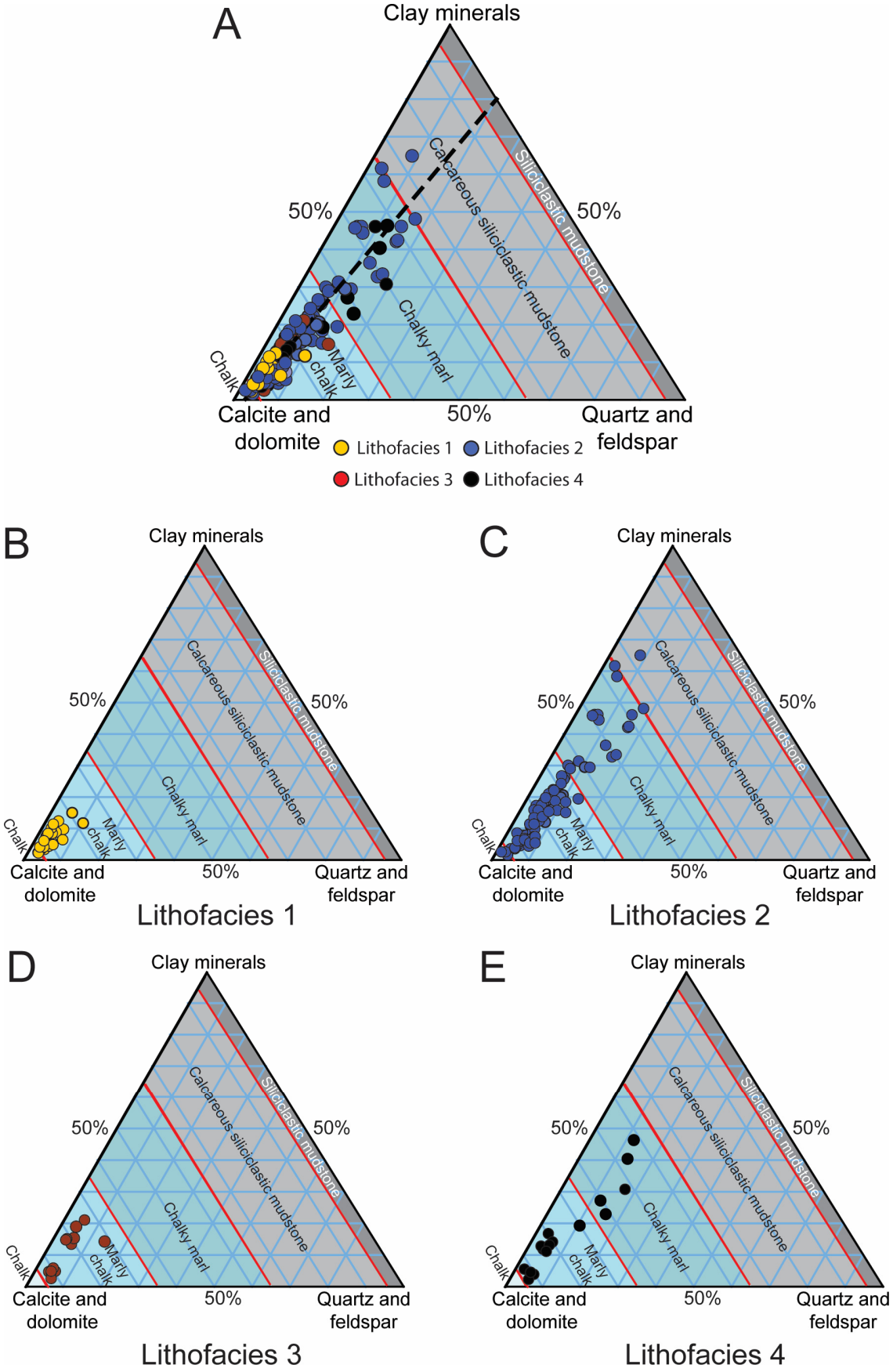

Figure 4. Plot of mineralogy using XRD data. (A) Mineralogical ternary diagram of all data where each analysis is identified by lithofacies type. The black-dashed line is an estimated trend line. (B) Mineralogical ternary diagram for lithofacies 1. (C) Mineralogical ternary diagram for lithofacies 2. (D) Mineralogical ternary diagram for lithofacies 3. (E) Mineralogical ternary diagram for lithofacies 4.

between well burrowed (typical of oxic to slightly dysoxic conditions) to well laminated (typical of anoxic conditions), which serves as a good visual indicator of the degree of oxygenation in the absence of more rigorous geochemical analyses.

Austin Chalk Stratigraphy in Area of Investigation

The Austin Chalk was deposited during the uppermost Turonian Stage into the lowermost Campanian Stage, a 9 to 10 million yr time period (Phelps et al., 2013; Lowery et al., 2014) (Fig. 1A). In the area of study, it overlies the Eagle Ford and Tuscaloosa groups and underlies the Taylor Group (Fig. 1A).

The internal stratigraphy of the Austin Chalk section in the study area is not well documented in the literature (Loucks et al., 2021b). Several non-peer-reviewed articles have published wireline logs with Austin Chalk stratigraphic picks and informal internal zonation, but rarely does the top Austin Chalk appear consistently correlated. In our experience, top Austin Chalk is rarely consistent between operatories either. Loucks et al. (2021b) addressed this problem for the western Louisiana area. In their figure 7, Loucks et al. (2021b) presented a wireline-log cross-section that displays several different tops for the Austin Chalk that are proposed in the literature. Based on two cored wells in Louisiana (core 5 in Table 1 and Figure 1C and another core [Marathon No. 1 Robert Todd] east of the study area), they picked the Austin Chalk top shown in the Chevron No. 1 Burton in Figure 2 as the top of the Austin Chalk section. This top is based on lithologic changes between the Austin Chalk and Taylor sections. Also, this top appears to capture the major section of interest within the Austin Chalk (e.g., Louisiana Mineral and Energy Board, 2018), as well as the section commonly cored in the Brookeland, Burr Ferry, Burr Ferry North, and Burr Ferry South fields. Therefore, the Austin Chalk top shown in Figure 2 serves as a functional working top for the Austin Chalk and it is correlatable in wells and cores (Figs. 2 and 3) in the study area. The base of the Austin Chalk is relatively straightforward to correlate (Fig. 2) and is, in general, consistently picked in the literature.

In the study area, the Austin Chalk has been informally divided into three units, A, B, and C, with C unit being the uppermost unit (e.g., Stamatedes, 2019). The A to C units are shown on the wireline cross-section in Figure 2 and in cores in Figure 3. The major target of interest within the Austin Chalk section appears to be unit A (e.g., Louisiana Mineral and Energy Board, 2018). In Figure 2, a zone labeled "volcanic-rich zone" appears on several wireline-log raster files and is noted to contain volcanic debris. It is a distinct zone that can be correlated over the present study area and into eastern Louisiana (Loucks et al., 2021b). On wireline logs, this zone is characterized by high gamma ray and spontaneous potential responses and low resistivity responses (Fig. 2). No preserved volcanic ashes were observed in this zone, but they may have been extensively altered to clay minerals. Lithofacies in this "volcanic-rich zone" are discussed below.

LITHOFACIES

Loucks et al. (2020b, 2021b) identified five basic lithofacies throughout the regional Austin Chalk trend. Four of the lithofacies were deposited more or less in-place (i.e., minor resedimentation) and the fifth lithofacies was deposited by gravity flows where the deposited sediments originated in another area (i.e., resedimentation events). These five lithofacies are the building blocks of the Austin Chalk stratigraphic sections and tend to create repeatable, larger-scale stacking patterns (Loucks et al., 2020b, 2021b). Each of these lithofacies are present in the area of investigation and are described below, then expanded upon with respect to mineralogical, organic-matter, and source-rock quality properties.

Lithofacies Descriptions

In-place lithofacies (lithofacies 1 through 4; Fig. 4) are all largely composed of similar deep-water biota with differences in fabric and bedding styles, mineralogy, and organic-matter content; in contrast, the gravity flow-related facies (lithofacies 5) contains some shallow-water biota mixed with deep-water biota. The predominant deeper-water biota consists of open-marine organisms that generally lived seaward of higher-energy, nearer-shore conditions on the outer shelf and/or slope. Planktic microorganisms including coccolithophores, planktic foraminifers, and calcispheres lived in the water column and make up the bulk of the rock composition. Inoceramid clams that lived in deeper-water, aerobic to dysaerobic muddy bottom environments (Boucot, 1990) are also present in varying abundances. Coccolith hash (i.e., fragments or elements of coccoliths) is the major component of the matrix in each lithofacies (Fig. 5). A review of these organisms as evidence for a deeper-water setting generally below storm wave base was presented for the Eagle Ford Group by Loucks (2018). The shallower-water biota introduced by resedimentation in the gravity flow-related lithofacies consist predominantly of oysters, echinoderms, benthic foraminifers, and ostracods.

Lithofacies 1 is a TOC–poor (mean TOC = 0.33 wt%), highly burrowed marly chalk (Figs. 6A, 6B, and 6F). It ranges in thickness from less than 1 ft (0.3 m) up to 15 ft (3 m) (Fig. 3). Most burrows are horizontal, but some are vertical to oblique. Trace fossils *Zoophycos* and *Thalassinoides* are most commonly observed. In addition to the abundant coccolith fragments, which form the majority of the matrix, planktic foraminifers (e.g., Fig. 6E) of several types are very common along with inoceramid fragments (e.g., Fig. 6E), calcispheres, and saccocomids (i.e., swimming crinoids). Minor amounts of shallower-water organisms include echinoderm plates and spines (e.g., Fig. 6E), ostracod valves, and oyster fragments. Extremely rare benthic foraminifers were noted.

Lithofacies 2 is a marly chalk to chalky marl with a wide range of present-day TOC content (mean TOC = 0.74 wt%, range = 0.21 to 2.99 wt%) (Figs. 6A, 6B, and 6F–6H). Although the biota are nearly identical to those observed in lithofacies 1, lithofacies 2 differs in burrow types and siliciclastic content. This lithofacies is strongly dominated by horizontal burrows and lacks vertical and highly oblique burrows, indicating greater environmental stress (e.g., low dysaerobic conditions) at the sediment-water interface than was present during lithofacies 1 deposition. The amount of siliciclastic content (~25%) in most samples in lithofacies 2 is much higher than the amount of siliciclastics (~10%) in lithofacies 1. As shown in Figure 4, the amount of siliciclastic material can range up to 60 wt% or more in some samples. Bed thickness ranges between less than 1 ft (0.3 m) to 85 ft (25.9 m) (Fig. 3).

Lithofacies 3 is a moderate TOC (mean TOC = 1.6 wt%), slightly burrowed, laminated marly chalk and lesser chalky marl (Figs. 7A, 7B, 7E, and 7F). It varies from well laminated to poorly laminated; the presence of laminae is important as they indicate lack of or low influence of bioturbation and generally imply dysoxic to anoxic bottom conditions (e.g., Arthur and Sageman, 1994). The laminations vary in skeletal content and mineralogy (Figs. 7E and 7F). The burrows, when present, are generally horizontal and small as compared to those in lithofacies 1 and 2. The observed biota (Figs. 7E and 7F) is similar to those in lithofacies 1 and 2, but generally lack any shallower-water fauna. Larger inoceramid fragments are preserved more commonly in this lithofacies than in lithofacies 1 or 2 given that the prismatic shells readily fragment along the crystal boundaries (e.g., Fig. 8B) and are easily disaggregated in more heavily bioturbated strata. Loucks et al. (2021b) found that larger inoceramid fragments correlated with lower rates of bioturbation (i.e., lower disturbance of the sediment). An interesting diagenetic

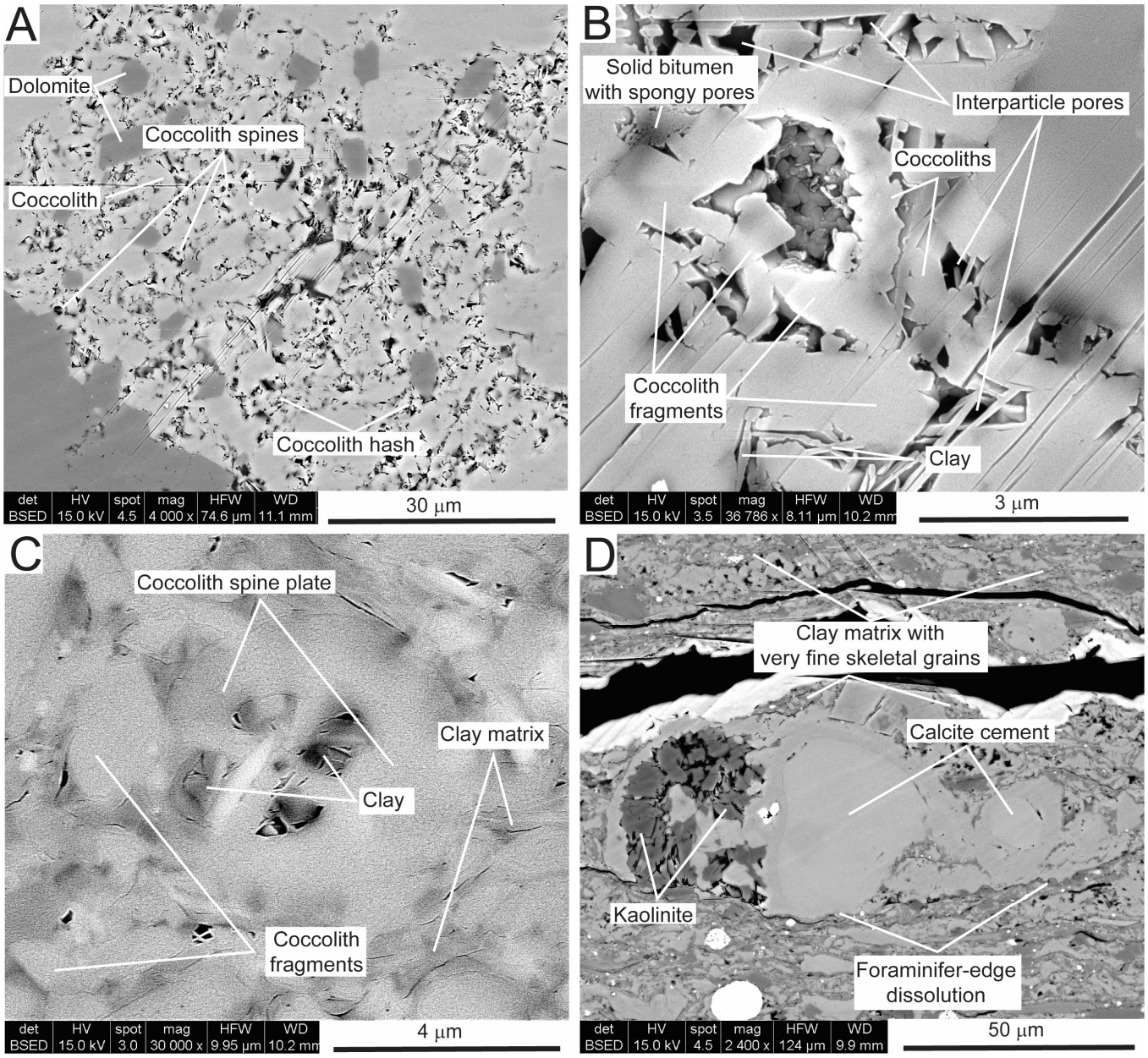

Figure 5. SEM images of matrix characteristics. (A) Lithofacies 3. Chalk matrix composed of coccoliths, coccolith spines, and coccolith fragments. Clay-mineral platelets occur in the interparticle pore spaces between very fine particles. Scattered anhedral dolomite crystals are present and are interpreted as detrital or reworked. No. 1 McShane Trust; 14,479.3 ft (4413.3 m). (B) Lithofacies 3. Close-up of coccolith matrix with clay minerals in some of the intraparticle pores. Some solid bitumen is present. No. 1 McShane Trust; 14,479.3 ft (4413.3 m). (C) Lithofacies 2. Coccolith spine plate and coccolith fragments with clay minerals in pores. No. 1 BP American A–187; 14,624.3 ft (4457.5 m). (D) Lithofacies 4. Foraminifer in coccolith and clay-mineral matrix. Sample shows laminations. Foraminifer displays dissolution along boundary adjacent to clay seam. Foraminifer chambers are filled with authigenic kaolinite and calcite cements. No. 1 BP American A–187; 14,531.0 ft (4429.0 m).

(FACING PAGE) Figure 6. Core slab and thin-section examples of lithofacies 1 and 2. (A) Lithofacies 1. Burrowed marly chalk. No. 1 ARCO Vastar Unit A–183; 8971.6 ft (2734.5 m). (B) Lithofacies 2. Horizontal, burrowed, chalky marl with abundant solution seams. No. 1 ARCO Fee A–246; 9618.5 ft (2734.5 m). (C) Lithofacies 1 overlying lithofacies 2. Lower part of core slab shows abundant horizontal burrows with clay seams in mottled marly chalk to chalky marl. Upper part of core slab also shows abundant burrows and is less argillaceous than the lower part. No. 1 ARCO Vastar Unit A–183; 8971.6 ft (2734.5 m). (D) Lithofacies 1 grading up into lithofacies 2. Lithofacies 1 contains some horizontal burrows. No. 1 ARCO Fee A–246; 9614.0 ft (2930.3 m). (E) Lithofacies 1. Planktic foraminifers, inoceramid fragments, and echinoid spines in a matrix of peloidal, argillaceous coccolith hash. No. 1 BP American A–187; 14,562.7 ft (4438.7 m). (F) Lithofacies 2. Marly chalk with abundant planktic foraminifers and inoceramid fragments in a matrix of argillaceous coccolith hash. No. 1 ARCO Vastar Unit A–183; 8948.6 ft (2727.5 m). (G) Lithofacies 2. Abundant planktic foraminifers and calcispheres in a matrix of argillaceous coccolith hash. A saccocomid fragment is present. No. 1 BP American A–187; 14,623.7 ft (4457.3 m). (H) Lithofacies 2. Planktic foraminifers in a matrix of argillaceous coccolith hash. A rare benthic foraminifer is present. No. 1 ARCO Vastar Unit A–183; 8985.5 ft (2738.7 m).

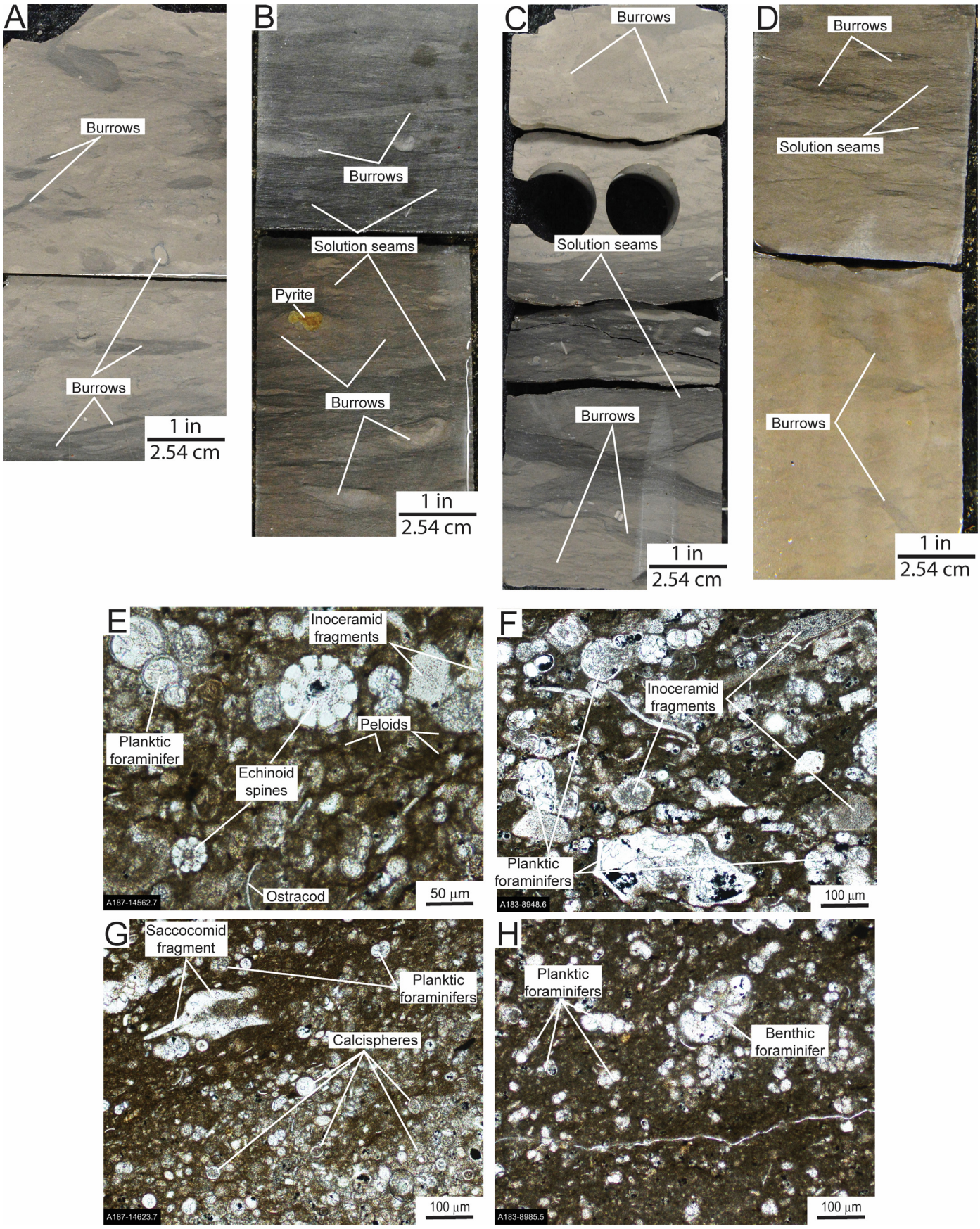
A
Burrows
Burrows
1 in
2.54 cm
B
Burrows
Solution seams
Pyrite
Burrows
1 in
2.54 cm
C
Burrows
Solution seams
Burrows
1 in
2.54 cm
D
Burrows
Solution seams
Burrows
1 in
2.54 cm
E
Inoceramid fragments
Peloids
Planktic foraminifer
Echinoid spines
Ostracod
A187-14562.7
50 µm
F
Inoceramid fragments
Planktic foraminifers
A183-8948.6
100 µm
G
Saccocomid fragment
Planktic foraminifers
Calcispheres
A187-14623.7
100 µm
H
Planktic foraminifers
Benthic foraminifer
A183-8985.5
100 µm

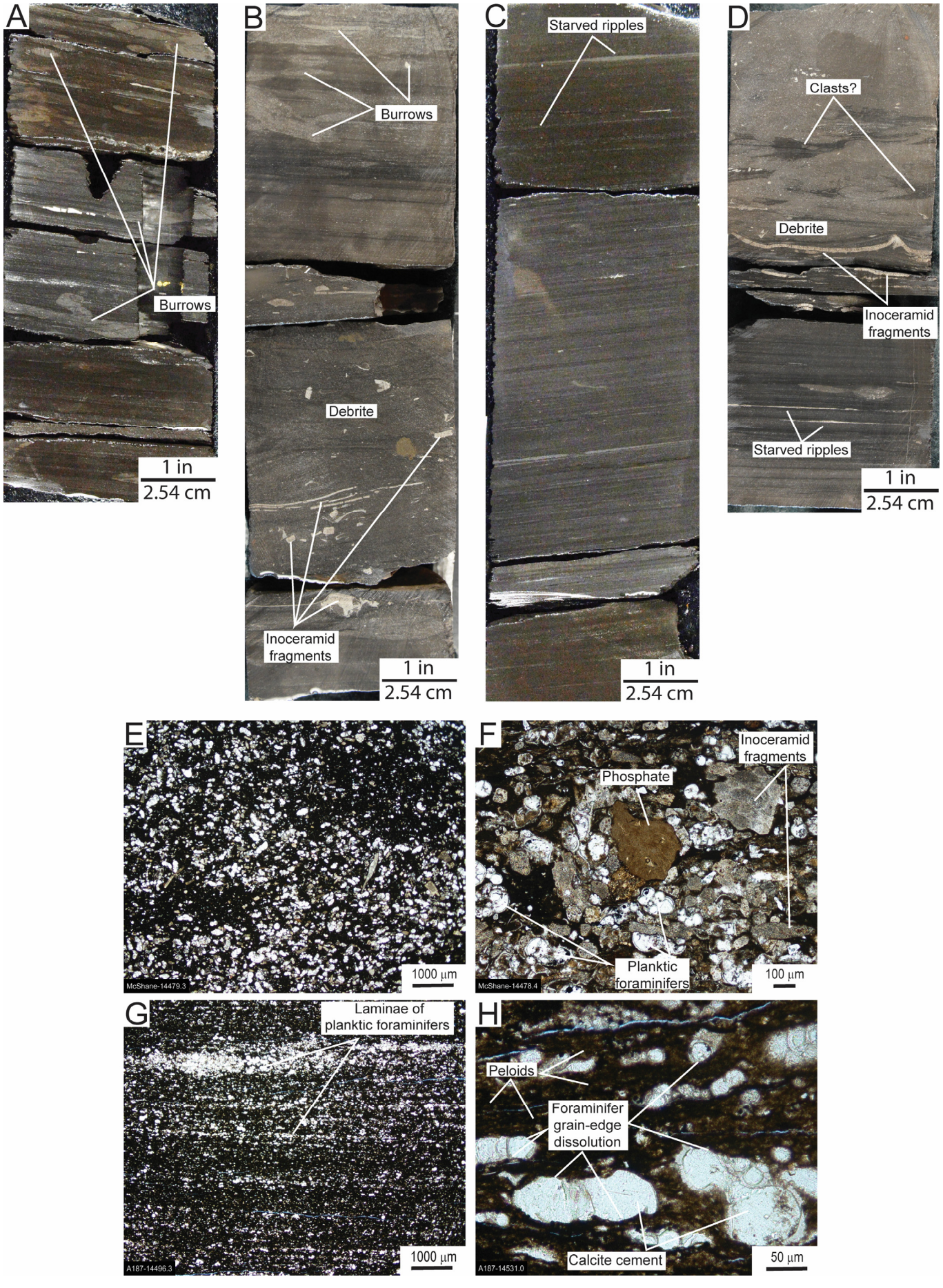
A
Burrows
1 in
2.54 cm
B
Burrows
Debrite
Inoceramid fragments
1 in
2.54 cm
C
Starved ripples
1 in
2.54 cm
D
Clasts?
Debrite
Inoceramid fragments
Starved ripples
1 in
2.54 cm
E
1000 µm
McShane-14479.3
F
Inoceramid fragments
Phosphate
Planktic foraminifers
100 µm
McShane-14478.4
G
Laminae of planktic foraminifers
1000 µm
A187-14496.3
H
Peloids
Foraminifer grain-edge dissolution
Calcite cement
50 µm
A187-14531.0

(FACING PAGE) Figure 7. Core slab and thin-section examples of lithofacies 3 and 4. (A) Lithofacies 3. Well-laminated marly chalk with some burrows. No. 1 BP American A–187; 14,528.5 ft (4428.3 m). (B) Lithofacies 3 overlying lithofacies 5 debrite. Scattered burrows in laminated marly chalk. Lower part of core slab is a debrite with inoceramid fragments. No. 1 McShane Trust; 14,477.5 ft (4412.7 m). (C) Lithofacies 4. Well-laminated marly chalk. Some laminae appear to be starved ripples. No. 1 BP American A–187; 14,498.0 ft (4419.0 m). (D) Lithofacies 4 underlying lithofacies 5 debrite. Lithofacies 4 is well-laminated with some starved ripples and rare burrows in a few layers. The debrite above has large inoceramid fragments at its base and very irregular (compacted and distorted) argillaceous mud clasts above. No. 1 McShane Trust; 14,477.5 ft (4412.7 m). (E) Lithofacies 3. Burrowed marly chalk with very fine skeletal grains. No. 1 McShane Trust; 14,479.3 ft (4413.3 m). (F) Lithofacies 3. Planktic foraminifers and inoceramid fragments in marly chalk. A phosphate grain is present. No. 1 McShane Trust; 14,478.4 ft (4413.0 m). (G) Lithofacies 4. Well-laminated marly chalk where laminae are alternating layers of planktic foraminifers and peloids. No. 1 BP American A–187; 14,496.3 ft (4418.5 m). (H) Lithofacies 4. The foraminifers in this sample display dissolution along their boundaries with the argillaceous matrix. The chambers of the foraminifers are filled with calcite cement. No. 1 BP American A–187; 14,531.0 ft (4429.0 m).

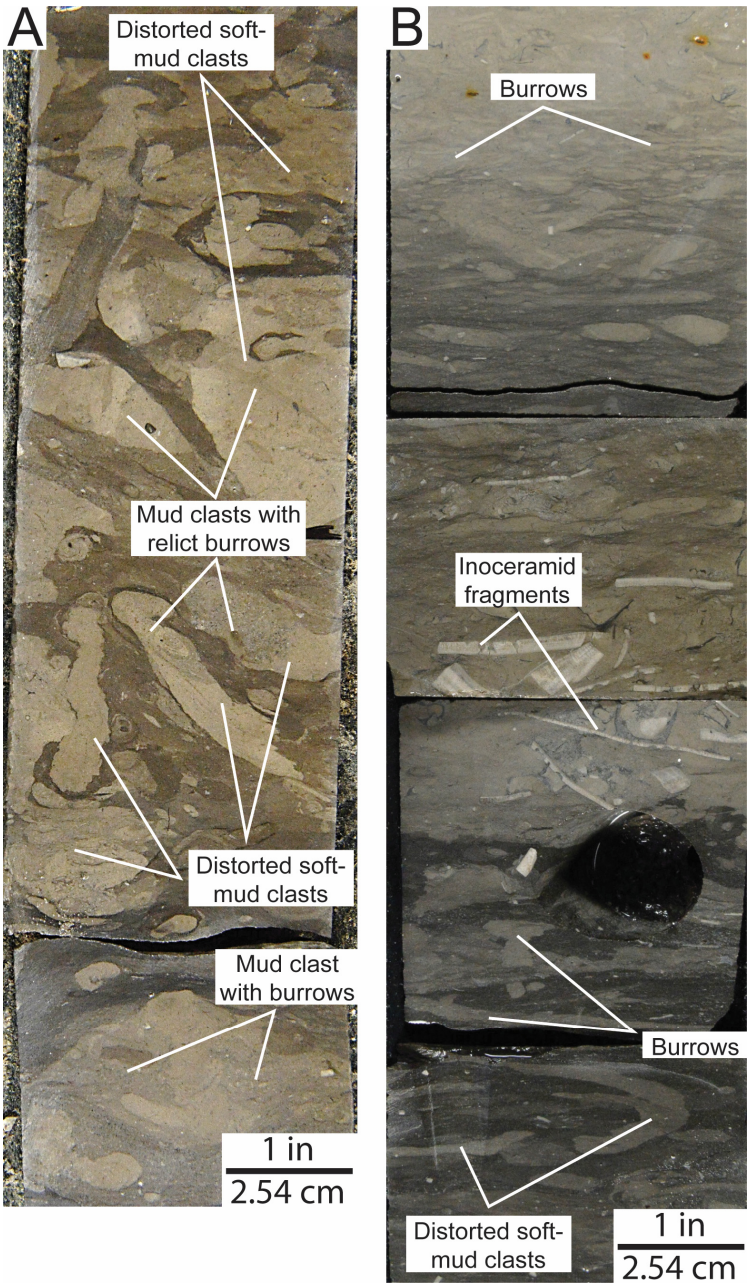

Figure 8. Core slab examples of lithofacies 5. (A) Lithofacies 5 debrite with distorted soft-sediment mud clasts. Several mud clasts show relict burrows. No. 1 ARCO Fee A–246; 9567.6 ft (2916.2 m). (B) Lithofacies 5 debrite showing vertical variation. The base has distorted soft-mud clasts overlain by a layer of large inoceramid fragments. The upper section is burrowed lithofacies 2 grading up into lithofacies 1. No. 1 ARCO Vastar Unit A–183; 8944.1 ft (2726.2 m).

feature in lithofacies 3 and 4 is the dissolution of the planktic foraminifers (Fig. 7H). This was also noted by Loucks et al. (2020b, 2021a, 2021b), who proposed that the dissolved calcium carbonate contributed to cementation within the Austin Chalk. Coccolith fragments are probably also being dissolved in the very argillaceous chalk, but because they are so fine grained, it is difficult to discern.

Lithofacies 4 is a TOC–rich (mean TOC = 2.03 wt%), well-laminated marly chalk to chalky marl displaying no bioturbation (Figs. 7C, 7D, 7G, and 7H). Loucks et al. (2020b, 2021b) determined that some of the black laminae formed as deep-water, anoxic microbial mats. The biota (Figs. 7G and 7H) is the same as in lithofacies 3. Large inoceramid fragments (i.e., width of the core or larger) are common (e.g., Fig. 7D).

Lithofacies 5 is relatively minor (occurs in 5 cores as thin beds from 1 to 4 times) in the area of investigation. These deposits are debrites composed of soft-sediment-mud clasts and inoceramid fragments (Fig. 8). The mud clasts contain relic burrows and the clasts are commonly distorted.

Mineralogy

In defining lithofacies types, mineralogy is a major factor. Five cores were analyzed for mineralogy using XRD analysis. The mineralogical data are plotted on a ternary diagram (Fig. 4) developed by Loucks et al. (2020b) for argillaceous chalks in the Gulf of Mexico. It is, in part, based on the work of Longman et al. (1998). The three endmembers (calcite and dolomite, clay minerals, and quartz and feldspar) emphasize the prominent differences in mineralogy of the Austin Chalk strata. The plots show XRD analyses delineated by lithofacies types. Note that lithofacies 1 plots at the calcite and dolomite apex (marly chalk) (Figs. 4B, 6A, 6B, and 6F); however, dolomite is relatively rare in the Austin Chalk strata (Loucks et al., 2020a). Lithofacies 2 has the widest spread of mineralogy ranging from 25% to 95% calcite (marly chalk to calcareous siliciclastic mudstone) (Figs. 4C, 6C–6E, 6G, and 6H). Lithofacies 3 plots as marly chalk (Figs. 4D, 7A, 7B, 7E, and 7F), whereas lithofacies 4 plots as marly chalk to chalky marl (Figs. 4E, 7C, 7D, 7G, and 7H). Lithofacies 5 was not sampled for XRD analysis. Some argillaceous and TOC–rich layers appear as thin (i.e., less than a few inches), TOC–rich mudstone stringers, but these are rare and are not treated as a well-defined lithofacies.

As pointed out by Loucks et al. (2020a, 2020b), the population trend of mineralogy is relatively linear (Fig. 4A; note black-dashed line) plotting between the calcite and dolomite apex and the clay-mineral apex. This mixing-line trend is interpreted to be related to changing carbonate productivity in the open-marine environment while siliciclastic input remained relatively constant. Input of siliciclastics into the open-marine setting was interpreted to be by aeolian processes (see Loucks et al. [2020a] for a detailed discussion). This mixing line is similar to what is observed in the XRD analyses of Austin Chalk cores from South Texas and the San Marcos Arch (Loucks et al., 2020a).

Organic-Matter and Source-Rock Quality

All cores in this investigation were sampled using HAWK and Rock-Eval pyrolysis and the results are plotted on a source-rock-quality diagram (Fig. 9A) and a pseudo–van Krevelen diagram (Fig. 9B) with descriptive statistics shown in Figures 9C–9E.

Average calculated vitrinite reflectance (R_o) from T_{max} values (Table 1) is 0.62% for cores north of the shelf edge and 0.92% for cores south of the shelf edge. The wide range in maturity estimation reflects the large range in average burial depth between strata north and south of the shelf edge (~8500 ft versus ~14,900 ft (2590 m versus 4540 m), respectively). The high-maturity rock samples south of the shelf edge appear to have lower apparent source-rock quality than expected (Figure 9A) because of their higher maturity related to burial depth. Loucks et al., (2021b) demonstrated that, in their Louisiana organic-matter analysis, samples with lower R_o values retained higher S1+S2 values and higher hydrogen-index levels indicating less transformation of original kerogen.

A plot of S1+S2 source-rock quality versus TOC (Fig. 9A) shows that many of the samples have fair to excellent amounts of TOC, but less optimal (poor to fair) S1+S2 values. Few samples have good to excellent S1+S2 values. The large amount of low (i.e., poor quality) S1+S2 values is also interpreted to be related to higher maturity levels experienced during deeper burial. Figure 9C tabulates mean TOC by lithofacies and displays a distinct relationship between lithofacies and amount of TOC (Fig. 9D). Lithofacies 1 has the lowest amount of TOC (0.33 wt%), whereas lithofacies 4 has the highest amount (2.03 wt%). Also, the strata north of the shelf margin have a lower mean TOC (0.71 wt%) as compared to the strata south of the shelf margin that have a higher mean TOC (1.04 wt%) (Fig. 9E). This contrast in amount of TOC across the margin is related to the higher abundance of TOC–rich lithofacies 3 and 4 south of the shelf margin as discussed above. The mean TOC value within each lithofacies does not vary significantly across the shelf margin (Fig. 9E). The best source-rock quality, in terms of abundance of TOC and type of organic matter, is found in lithofacies 3 and 4 and some of lithofacies 2 (Fig. 9). These lithofacies are dominated by type II kerogen with TOC values of 1 wt% or greater (Fig. 9). The clear relationship between lithofacies and TOC preservation observed here is similar to what Loucks et al. (2020a, 2021b) found along the Austin Chalk trend from the Texas-Mexico border into Louisiana.

The higher thermal maturation is also expressed in the pseudo–van Krevelen diagram (Fig. 9B) as indicated by the relatively low hydrogen index values (i.e., less than 200mg HC/g TOC) for most of the samples. The initial kerogen was likely a mixture of type II and lesser type III as is seen in many other Austin Chalk cores (e.g., Loucks et al., 2020b, 2021b).

LITHOFACIES VARIATIONS AND STACKING PATTERNS

Vertical lithofacies variations and stacking patterns were described for all cores in the study area. Two core-based cross-sections were constructed: an oblique dip section north of the shelf margin (cross-section C–D), and a strike section south of the shelf margin (cross-section E–F) (Figs. 1C and 3). As seen in the cross-sections, most of the core coverage in each well is 50% or less of the full Austin Chalk section. The updip, onshelf cross-section shows good coverage of unit A and the volcanic-rich zone, whereas the downdip, upper slope cross-section shows good coverage of unit B and volcanic-rich zone and fair coverage of units A and C . The lack of complete core coverage of the entire Austin Chalk section hinders an in-depth analysis of lithofacies stacking patterns; however, some initial conclusions about lithofacies stacking patterns and regional distribution can be established.

Onshelf Cross-Section C–D

The onshelf cross-section C–D consists of four core descriptions, three of which cover only the Austin Chalk unit A and volcanic zone, and one of which incompletely covers unit A through C. The Austin Chalk onshelf lithofacies along cross-section C–D are uniform throughout the section indicating similar, laterally continuous environment conditions during deposition. Bioturbation is the dominant sedimentary process observed and variations in the amount of argillaceous material controlled whether lithofacies 1 or 2 was deposited.

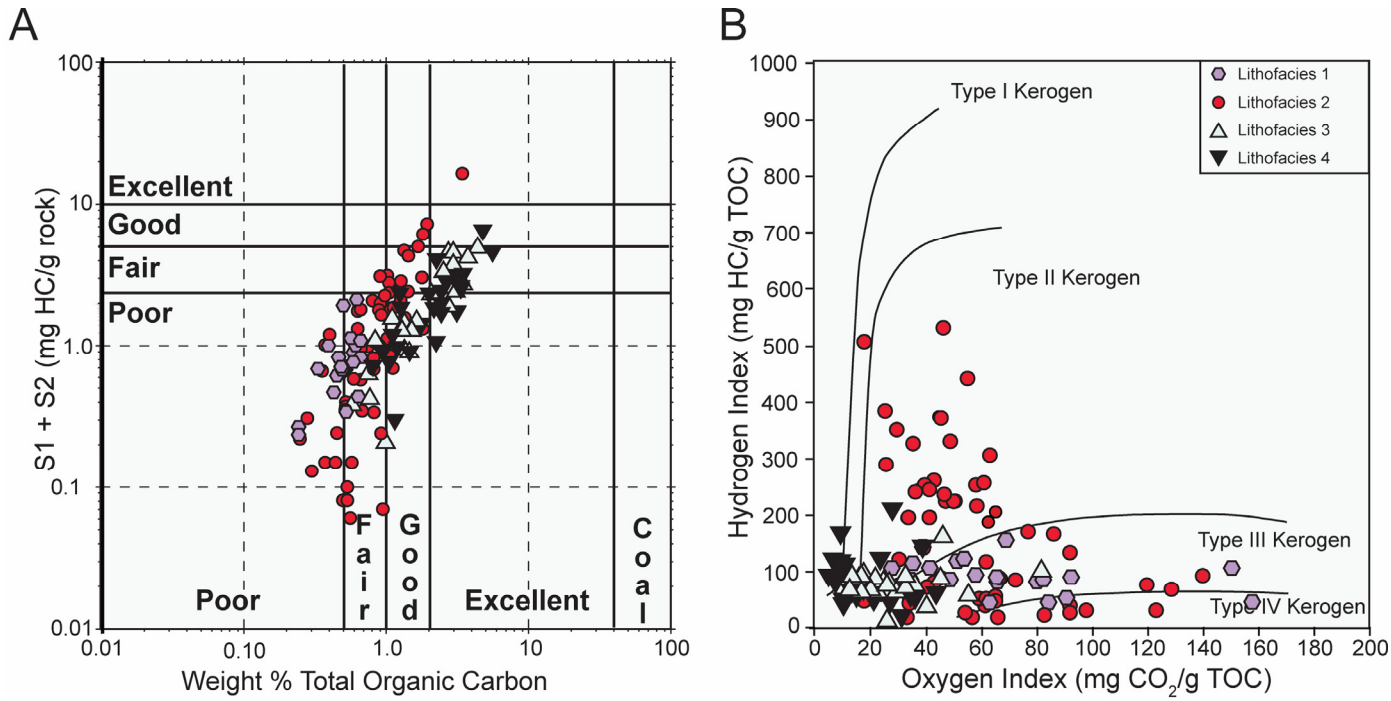

C

	Mean	Std. Dev.	Count	Minimum	Maximum
TOC (wt%) All lithofacies	0.97	0.85	263	0.10	4.99
TOC (wt%) Lithofacies 1	0.33	0.16	58	0.10	0.70
TOC (wt%) Lithofacies 2	0.74	0.49	122	0.21	2.99
TOC (wt%) Lithofacies 3	1.60	0.2	42	0.33	3.98
TOC (wt%) Lithofacies 4	2.03	1.01	36	0.26	4.99

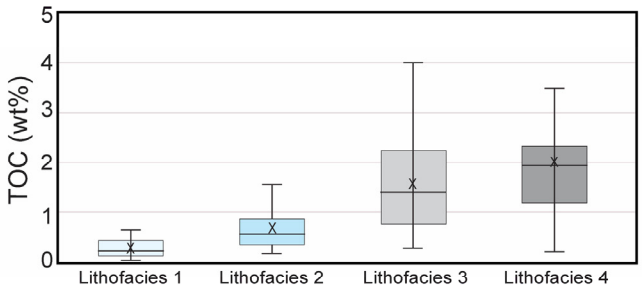

E

	Mean	Std. Dev.	Count	Minimum	Maximum
TOC (wt%) Onshelf Lithofacies 1	0.24	0.12	32	0.10	0.70
TOC (wt%) Onshelf Lithofacies 2	0.87	0.40	40	0.25	1.84
TOC (wt%) Onshelf Lithofacies 3	0.90	0.14	4	0.75	1.01
TOC (wt%) Onshelf Lithofacies 4	2.70	0.76	3	1.83	3.26
TOC (wt%) Onslope Lithofacies 1	0.45	0.14	24	0.16	0.64
TOC (wt%) Onslope Lithofacies 2	0.52	0.24	54	0.21	1.27
TOC (wt%) Onslope Lithofacies 3	1.77	1.06	23	0.44	3.98
TOC (wt%) Onslope Lithofacies 4	2.20	1.08	20	1.05	4.99

Figure 9. Source-rock quality analysis. (A) TOC versus S1+S2 plot displaying source-rock quality. Datapoints are assigned lithofacies identifiers. (B) Pseudo–van Krevelen plot showing kerogen types. The data appear to have been affected by thermal maturation associated with burial. (C) Descriptive statistics of TOC separated by lithofacies. (D) Box plot showing differences in TOC abundance by lithofacies. Box = interquartile range; horizontal line in box = median; X = mean; and vertical line = minimum to maximum range. (E) Descriptive statistics of mean TOC separated by lithofacies that were deposited onshelf and upper slope.

Intervals of unit A recovered in all cores are fairly similar, with alternating beds of lithofacies 1 and 2. A single debrite (lithofacies 5) was recorded in core 3. As unit A is predominantly composed of heavily burrowed lithofacies, a well-oxygenated environment with good living conditions for infaunal, seafloor-dwelling organisms can be inferred.

The volcanic-rich zone is again composed of lithofacies 1 and 2. Some debrites (lithofacies 5) are present in cores 3 and 4. Wells 3 and 4 are close together (Fig. 3A) and the debrites in the two wells may be related. Two thin beds of lithofacies 3 are present in core 6. No evidence of volcanic ashes were noted in cores from this unit; however, the wireline logs suggest possible altered or bioturbated ash beds as indicated by spontaneous potential, gamma ray, and resistivity spikes. Bioturbation is the dominant sedimentary feature in this unit, which again indicates fair to good living conditions for bottom infaunal dwellers.

Units B and C were almost completely cored in well 5, and a small interval of unit B was cored at the base of core 4. The complete section alternates between beds of lithofacies 1 and 2, with a single thin bed of lithofacies 3 documented in unit B. The contact with the Taylor Group above is based on wireline logs and a change from thinner beds in lithofacies 1 and 2 in Austin Chalk unit A to thicker beds in lithofacies 1 and 2 in the Taylor Group. Again, this section is dominated by bioturbation and varying amounts of argillaceous material. These lithofacies suggest fair to good living conditions for bottom infaunal dwellers.

Upper-Slope Cross-Section E–F

There is a strong contrast in lithofacies abundance and stacking patterns between the onshelf and upper-slope environments. While the onshelf area is dominated by alternating beds of lithofacies 1 and 2 (Fig. 3A), the upper-slope area is more variable in lithofacies distribution both vertically and laterally (Fig. 3B). The upper-slope cross-section E–F contains a mix of all four in-place lithofacies as well as some occurrences of lithofacies 5.

Unit A varies laterally from west to east, with a greater amount of lithofacies 3 and 4 in the section to the east and a greater amount of lithofacies 2 to the west. No lithofacies 1 was recorded in available cores in unit A. The western-most core in unit A (core 2) is a uniform section of lithofacies 2 indicating fair to good bottom conditions for infauna. The next core to the east (core 8) encountered a slide block that appears to have affected unit A and unit B (no core was recovered from unit C). The strata in this core is tilted and deformed with some clasts developed from deformation. In cores 7 and 10, the most eastern cores, there is a change from predominantly lithofacies 2 to cycles of lithofacies 2 mixed with lithofacies 3 and 4 (Fig. 3B). These cycles generally have sharp contacts indicating fairly rapid changes in environmental conditions. Cycles such as these in the Austin Chalk have been suggested by Loucks et al. (2020b, 2021b) to be caused by climatic cycles associated with orbital relationships between the Earth and the Sun (i.e., Milankovitch cycles). Locklair and Sageman (2008) determined that a similar process produced cycles in the age-equivalent Niobrara Group in the Western Interior Seaway as did Eldrett et al. (2015) for the cycles observed in the Eagle Ford Group below the Austin Chalk.

The volcanic-rich zone displays the same west to east lithofacies transition seen in unit A. Lithofacies 2, with some lithofacies 1, in the west transitions into cycles of lithofacies 2 with lithofacies 3 and 4 in the east (Fig. 3B). Again, the cycles in cores 7 and 10 show sharp contacts, indicating rapid changes in bottom-water conditions. No unaltered volcanic ashes were recognized in these cores.

Unit B displays vertical heterogeneity, with the base of the unit dominated by lithofacies 1 and 2 and upsection intervals comprised of cyclic, interbedded lithofacies 1–4. The uniform burrowed lithofacies in the lower part of unit B suggests fair to good living conditions at the sea bottom, while the cyclic upper section of unit B suggests living conditions of variable quality punctuated by episodic deoxygenation of bottom waters. Unit C shows an upward continuation of the cyclic stacking patterns with little variation in lithofacies from those documented in the upper unit B. It is interesting to note that, in unit B in the No. 1 BP American A–187 core, three thin (less than 1 cm) ash layers are present indicating some volcanic ashes reached this part of Texas.

MICROPETROGRAPHY OF THE AUSTIN CHALK STRATA

SEM analysis of selected samples of extremely fine-grained Austin Chalk strata predominantly composed of skeletal fragments of microorganisms facilitated greater insight into the micropetrography of the formation and the conditions extant during deposition and subsequent diagenesis. Rock texture, fabric, and mineralogical elements were described using this improved characterization methodology.

Texture

In the Austin Chalk strata, grain size and roundness are controlled by the original size, shape, and internal structure of the coeval organisms. It is important to distinguish grain roundness as an inherent biological feature versus a product of mechanical abrasion as these can have implications for the interpretation of depositional conditions. Foraminifers and calcispheres (Fig. 10) have rounded bodies and therefore, grain roundness is a biologically controlled property. Other grains such as coccolithophores and inoceramids are prone to fragmentation; consequently, grain size and roundness are also a function of broken fragments of these organisms and the subsequent impact of mechanical abrasion upon those fragments (Fig. 10).

Some internal sorting is produced by bottom-current traction flow resulting in laminae in lithofacies 3 and 4. By contrast, in lithofacies 1 and 2, bioturbation generally produces well-blended textures (i.e., homogenous). The chalks commonly show a bimodal grain-size distribution in all lithofacies (Fig. 10). The fine particles of coccolith matrix hash and clay minerals contrast with the larger microfossils, such as foraminifers, inoceramids, and calcispheres, and some siliciclastic mineral grains.

Fabric

Rock fabric provides critical insight into depositional processes and environmental conditions, but also impacts mechanical rock properties. The two dominant fabric groups in the Austin Chalk are burrowed lithofacies 1 and 2 (Figs. 6, 10A, and 10C) and laminated lithofacies 3 and 4 (Figs. 7, 10B, and 10D). The bioturbated fabric is predominantly composted of horizontal to low-angle burrows, but, lithofacies 1 does display some oblique to vertical burrows.

In contrast, the laminated lithofacies 3 and 4 have few to no burrows. The lack of bioturbation preserved laminations that are related to gravity flow or bottom-current processes. The laminations at SEM scale are not distinct layers, but rather are the product of slightly diffuse interlayers of very fine clay minerals and coarser grains (Figs. 10B and 10D). Elongated, bedding-parallel grains (Fig. 10B) emphasize the laminar fabric. Pressure solution also enhances the general laminated fabric, but the resulting clay seams are commonly anastomosing (Fig. 10D).

Mineral Components from Micropetrography

The Austin Chalk is a mixture of carbonate and siliciclastic components (Fig. 4). According to Longman et al. (1998), pure chalks are 95% or more carbonate. Rarely is the carbonate content greater than 90% in the Austin Chalk strata; as a result, it is important to assess the component mineralogy to understand the composition of the rock and its associated mechanical properties.

Calcite is the dominant mineral in most samples averaging 66.6% of total rock volume (range = 40.5 to 93.6%). The calcite is a product of bioproduction and coccolithophores are the most abundant source. Some calcite cement forms between coccolith elements in interparticle pores (Fig. 5) and as pore-filling cements in the intraparticle pores of foraminifers (Figs. 5D, 6E, 6F, 7E, and 7F) and calcispheres (Fig. 10A). Calcite cement may be sourced from the dissolution of foraminifers in lithofacies 3 and 4 where the calcite foraminifers are in contact with clay-mineral seams (Fig. 7H) as carbonate dissolution is pronounced at the observed calcite-clay mineral contact. Dolomite (Fig. 10A) is relatively uncommon (mean = 0.2%; range = 0 to 1.3%) and, in some examples, it appears to be detrital with later diagenetic overgrowths.

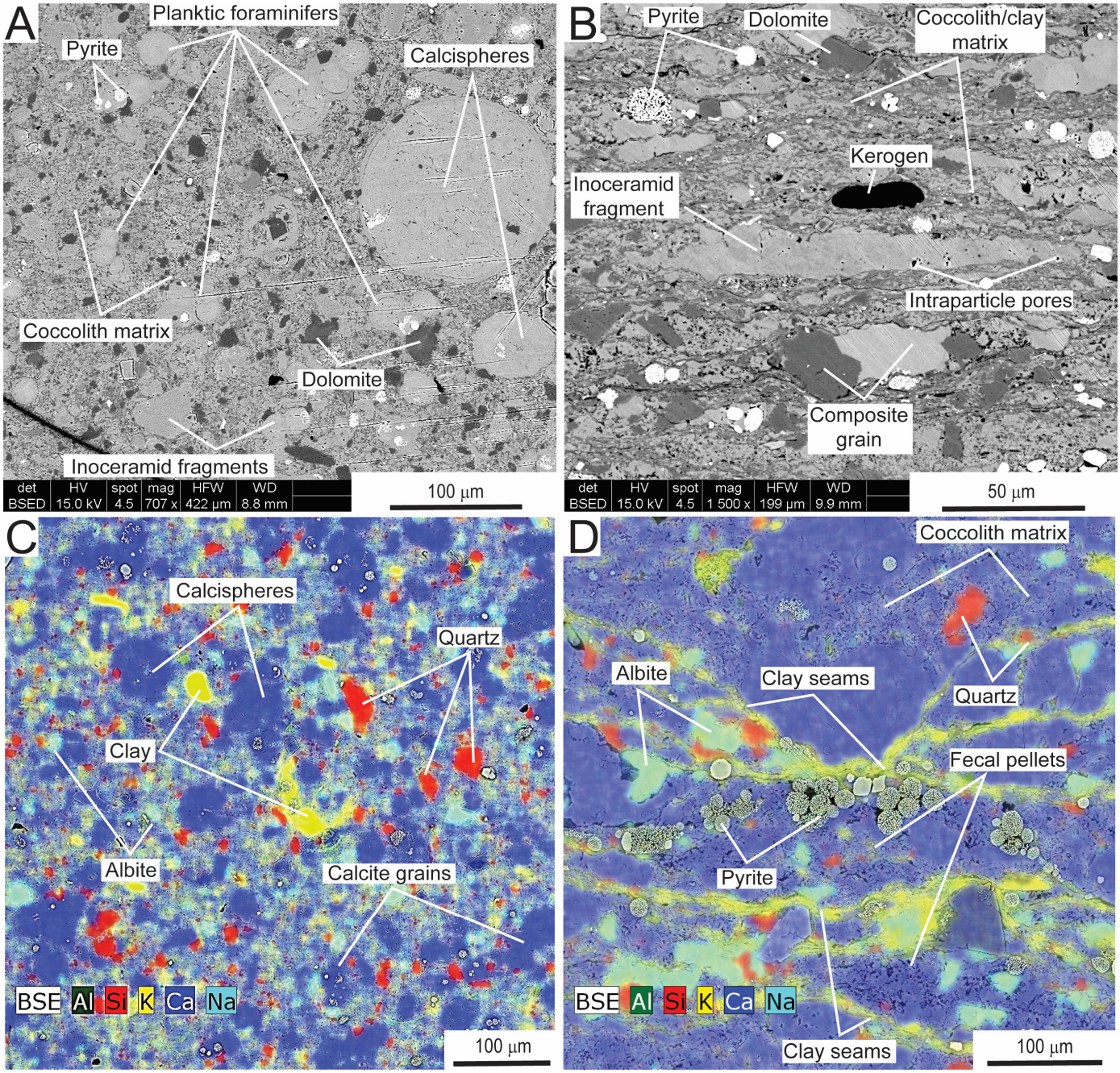

Figure 10. Micropetrography analysis images. (A) SEM backscatter image of marly chalk from lithofacies 2. The bimodal texture is a result of larger planktic foraminifer, calcisphere, and inoceramid grains mixed into a matrix of argillaceous coccolith hash. Abraded detrital dolomite crystals are present. Random orientation of the grains is likely caused by bioturbation. No. 1 BP American A–187; 14,624.3 ft (4457.5 m). (B) SEM backscatter image of laminated lithofacies 4 with elongate inoceramid fragment and composite grain. This sample also shows a bimodal texture with larger microfossils in a very fine-grained argillaceous coccolith hash. A large piece of type III (woody) kerogen is present. No. 1 BP American A–187; 14,531.0 ft (4429.0 m). (C) SEM–EDS image of lithofacies 2 showing highly bioturbated fabric. No. 1 BP American A–187; 14,624.3 ft (4457.5 m). (D) SEM–EDS image of lithofacies 4 showing clay seams and a layer of pyrite microframboids. Several fecal pellets composed of coccolith fragments are present, possibility produced by copepods. No. 1 McShane Trust; 14,467 ft (4409.5 m).

Quartz and feldspar grains are present, but are minor relative to grain volume. Quartz (mean = 6.2%; range = 2.5 to 11.9%) ranges in size from clay to very fine silt with rare larger grains (Figs. 10C and 10D). Albite (Figs. 10C and 10D) has a mean abundance of 2.1% (range = 0 to 3.2%) and K–feldspar is very rare with a mean abundance of 0.3%. These terrestrially sourced grain types are likely rare in this study area because of its position on the far distal edge of the shelf, over 100 mi (160 km) away from the nearest landmass.

Clay minerals consist predominantly of detrital smectite-illite (possibly volcanic in origin), but some are the result of diagenesis, such as the kaolinite that precipitated in the tests of foraminifers (e.g., Fig. 5D). Some clay minerals between coccolith elements (Figs. 5A and 5B) may also be diage-

netic, but it is difficult to differentiate diagenetic clay and detrital clay.

Pyrite is a commonly observed diagenetic mineral, especially in lithofacies 3 and 4, that is interpreted to be deposited in the sediment under dysoxic to anoxic conditions in the Austin Chalk strata (Loucks et al., 2020b, 2021b). Its most common habit is microframboidal (Figs. 10B and 10D). In XRD analyses, it ranges in abundance from 0.7 to 19.6% and has a mean of 5%. Also, phosphate occurs rarely in the samples as sand-sized grains (e.g., Fig. 7F).

MECHANICAL ROCK PROPERTIES

All three wells analyzed for UCS are located south of the shelf edge on the upper slope and contain all lithofacies types (Figs. 1C and 11). Analysis of each core shows acute and rapid changes in UCS readings at the foot-scale, indicating strong, fine-scale, mechanical-stratigraphic heterogeneity. Some of the marked changes correspond to documented lithofacies changes, but some changes show no correspondence, indicating this method of stratal analysis shows changes not readily defined by visual description. The importance of these changes is that they will affect the vertical propagation of fractures, which must be taken into consideration when planning a hydraulic fracturing program in a well.

A 10–point moving average of the UCS data breaks out thicker and coarser trends in rock properties (Fig. 11). These coarser packages further underscore how heterogeneous the Austin Chalk section is and enhance the concept that the Austin Chalk is not a simple, uniformly deposited chalk, but a complex rock unit composted of a variety of lithofacies with different mechanical properties.

The box plot associated with each core and the summary box plot of all UCS data indicate that the majority of UCS variations are correlative with lithofacies. Lithofacies 1 and 2 are generally similar in mean UCS values indicating a higher rock strength, whereas lithofacies 3 and 4 have overall lower rock strength values. Lithofacies 5 is similar to lithofacies 1 as it is homogenous and, in general, has lower TOC and argillaceous content. The major difference between lithofacies 1 and 2 relative to lithofacies 3 and 4 is that the former are highly bioturbated and the latter are laminated. One might conclude that the argillaceous content, TOC, or porosity would be controlling factors on mechanical strength, but in the Austin Chalk, lithofacies 1 and 3 have similar ranges of clay minerals abundances (Fig. 4), while lithofacies 2 and 4 have different ranges of clay minerals abundances. Porosity is very low in all lithofacies; therefore, clay and porosity do not appear to be the major controlling factors on UCS.

Variation in rock fabric between bioturbated (homogenous) and laminated (heterogenous) is likely a major controlling factor on rock strength. The fine laminations provide possible horizontal planes of weakness that reduce rock strength. Also, there is a contrast in TOC richness in the samples that have both UCS and TOC analyses (Fig. 12B). The laminated lithofacies 3 and 4 are richer in TOC than the burrowed lithofacies 1 and 2. The organic matter may have some negative effect on rock strength as shown in Figure 12A where TOC is plotted against UCS. There is a fair correlation between higher abundance of TOC and lower USC values.

RESERVOIR QUALITY

The pores in the Austin argillaceous chalk are generally in the nanometer range with only a few of the pores in the micrometer range (Figs. 5A, 5B, and 13A–13C). The dominant pore type, using the mudrock pore classification by Loucks et. al. (2012), is interparticle nanopores between coccolith elements and clay platelets (Figs. 5A, 5B, and 13A–13C). These interparticle pores tend to become cemented by calcite during burial as shown in Figure 13C. Figure 13A is an example where calcite cementation has bound several coccolith elements together making it difficult to distinguish individual elements. Intraparticle nanopores are not uncommon and occur mainly in inoceramid fragments (Fig. 13B), coccolith spines (Fig. 13A), and clay platelets (Figs. 5A–5C, 13A, and 13C). Intraparticle pores in foraminifers are generally cemented by calcite. Formation of solid bitumen occurred in cores that were buried into the oil window (R_o >0.6%). In all the present cores, spongy, organic-matter-filled pores (Fig. 13C) developed in the solid bitumen.

MGE porosity and permeability analyses were conducted on plugs in the study area (Fig. 13B). The plot of porosity versus permeability shows a good relationship between the two parameters (Fig. 13D). The principal conclusion from the MGE analysis is that reservoir quality is very low in argillaceous chalks where the mean porosity is 5.8%, with a range of 0.9 to 9.6%, and the geometric mean permeability is 285 nd, with a range of 6 to 2622 nd (Fig. 13B).

In a regional trend-wide analysis of Austin Chalk porosity and permeability using MGE analyses, Loucks and Peng (2021) found a good relationship between lithofacies and reservoir quality, with lithofacies 1 (containing the least amount of argillaceous material) having the highest reservoir quality and lithofacies 4 having the lowest reservoir quality. In the MGE sample population for this investigation, only one successful analysis was completed on lithofacies 4 as it is prone to fragment while drilling a plug. As a result, lithofacies 4 is not used in the reservoir-quality versus lithofacies discussion. This investigation did not find as strong a correlation between lithofacies and reservoir quality as Loucks and Peng (2021) did in their regional Austin Chalk reservoir quality analysis. In the present study, the mean porosity difference between the three lithofacies is only 0.5 porosity units, the mean permeability difference between the three lithofacies is 177 nd, and the geometric mean permeability between the three lithofacies is 79 nd (Figs. 13C and 13D). Overall, lithofacies in the population sampled do not appear to have a strong relationship to porosity and permeability; the three different lithofacies sampled are not strikingly dissimilar in reservoir quality.

DISCUSSION ON OPTIMAL LANDING ZONES OF HORIZONTAL WELLS

As addressed throughout this investigation, the argillaceous chalks that make up the Brookeland and Burr Ferry fields are complex because of their variation in lithofacies and associated rock properties. Having described the variation of lithofacies subregionally across the shelf margin and vertically within the Austin Chalk section, one must then consider how these variations impact reservoir characteristics, especially source-rock quality, reservoir quality, and mechanical properties, when deciding what section of the Austin Chalk is best to land a horizontal well.

As shown in cross-section C–D (Fig. 4A), the strata north of the shelf margin are predominantly composed of lithofacies 1 and 2, facies that are both well burrowed and internally homogeneous. The UCS and reservoir quality of these two lithofacies are similar although mineralogy and TOC content can vary. Overall, given these observations, there does not appear to be an optimal zone to land a horizontal well. The Stonegate No. 1 (5) core in Figure 4A is an example of the complete, relatively homogeneous Austin Chalk section.

South of the shelf margin on the upper slope, there is a distinct vertical transition in lithofacies (Fig. 4B). The lower Austin Chalk stratigraphic section is predominantly lithofacies 1 and 2, but with an increase in laminated lithofacies 3 and 4 to the east. The upper stratigraphic section on the upper slope is predominately cycles of lithofacies 1 and 2 with lithofacies 3 and 4. This change in lithofacies stacking patterns presents a decision point on where to land a horizontal well. Both the lower and upper

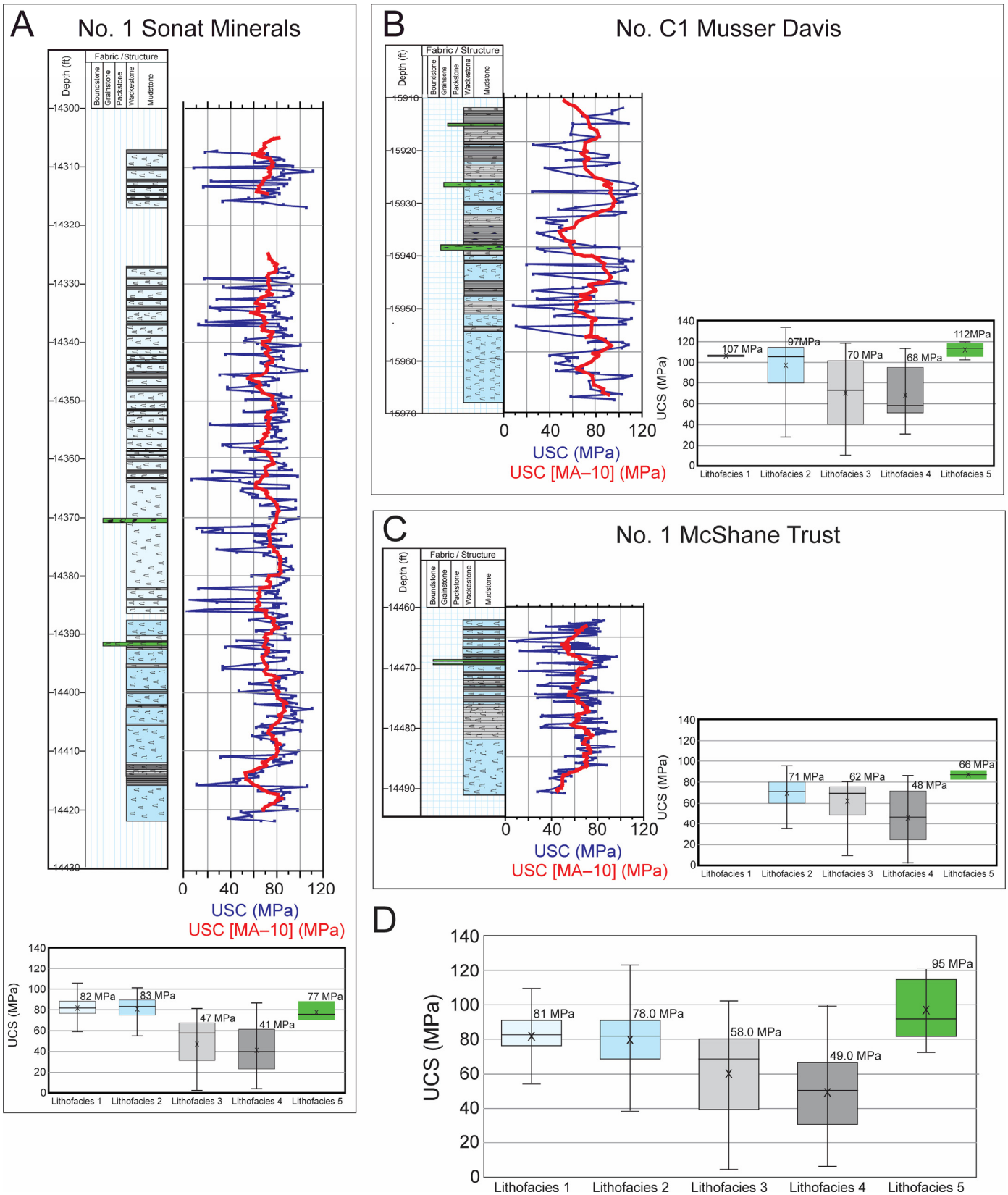

Figure 11. Unconfined compressive strength (UCS) data. For each of the three cores in this figure, a core description is presented along with the UCS profile of the raw data (blue line) and the 10–point moving average (red line). A box plot of descriptive statistics is also provided. Box = interquartile range; horizontal line in box = median; X = mean (the number is the digital mean); and vertical line = minimum to maximum range. (A) UCS data from the No. 1 Sonat Minerals core (core 7). (B) UCS data from the No. C1 Musser Davis core (core 9). (C) UCS data from the No. 1 McShane Trust core (core 1). (D) Summary box for all UCS data separated by lithofacies.

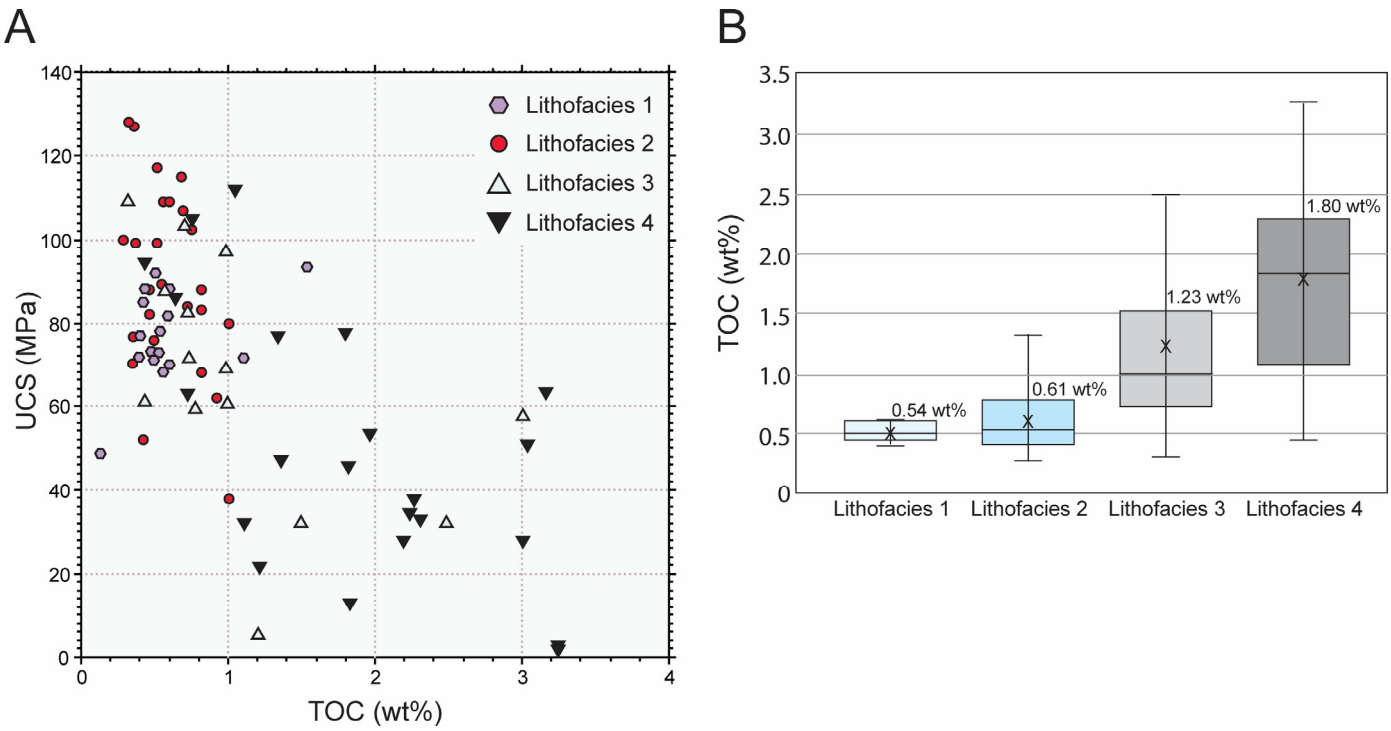

Figure 12. Plots relating total organic carbon to unconfined compressive strength (UCS). (A) TOC versus UCS. A reasonable correlation is shown between the two parameters. (B) Box plot of TOC separated by lithofacies for samples that have both TOC and UCS analyses. Box = interquartile range; horizontal line in box = median; X = mean (the number is the digital mean); and vertical line = minimum to maximum range.

sections on the upper slope have favorable, but different parameters for targeting. The lower section is more mechanically brittle (i.e., higher UCS values) and may be more prone to fracturing either naturally or artificially. However, it is lower in source-rock quality as compared to the upper section. This is important as the lower section would not be a strong candidate for the self-sourcing of hydrocarbons, as is commonly observed in unconventional reservoirs, and would instead require hydrocarbon migration to charge the section. The upper section, which has abundant beds of lithofacies 3 and 4 that are rich in organic matter, should be self-sourcing at higher thermal maturation burial depths. However, lithofacies 3 and 4 are mechanically weaker than lithofacies 1 and 2 and may not fracture as extensively. Also, the strong heterogeneity associated with the interbedding of the burrowed and laminated lithofacies may restrict fracture height and extent.

CONCLUSIONS

This investigation of the Austin Chalk reservoir in Brookeland, Burr Ferry, Burr Ferry North, and Burr Ferry South fields in the Sabine area of far East Texas and western Louisiana is important in that it provides new insights into the lithologic controls impacting these large hydrocarbon reservoirs. Four distinct in-place lithofacies and one transported lithofacies (i.e., debrites) are defined and discussed relative to other properties important for hydrocarbon production. Lithofacies 1 and 2 marly chalks and chalky marls are intensely burrowed, indicating oxic to slightly dysoxic conditions during deposition, whereas lithofacies 3 and 4 marly chalks and chalky marls are well laminated and have few to no burrows, indicating dysoxic to anoxic bottom-water conditions. Debrites attributed to lithofacies 5 were transported and are characterized by soft-mud clasts and large fragments of inoceramids. All lithofacies are argillaceous and lithofacies 3 and 4, along with some of lithofacies 2, have elevated TOC content, giving them greater self-sourcing potential for hydrocarbons.

Source-rock quality is strongly associated with lithofacies and reflects the degree of oxygenation in the depositional environment. Lithofacies 1 has the lowest source-rock quality whereas lithofacies 4 has the highest source-rock quality. The upper part of the upper slope section is organic-matter rich and is likely contributing to the hydrocarbon charge of the Austin Chalk reservoirs through self-sourcing.

Rock strength is also correlatable to lithofacies, with lithofacies 1 and 2, and lithofacies 3 and 4, being of similar integrity, respectively. The difference in rock strength between lithofacies 1 and 2, and lithofacies 3 and 4, appears to be related to sedimentary fabric; lithofacies 1 and 2 are largely homogeneous and lithofacies 3 and 4 are predominantly laminated. These differences may affect fracturing potential, as lithofacies 1 and 2 are more mechanically competent and, therefore, more brittle, than lithofacies 3 and 4.

Porosity is predominantly related to interparticle pores between coccolith fragments, but some intraparticle pores are present in inoceramid fragments and clay platelets. The interparticle pores are commonly segmented by clay platelets, which reduces pore-throat size and, consequently, permeability. Overall, the Austin Chalk reservoirs have low porosity and low permeability (mean porosity = 5.8% and geometric mean permeability = 285 nd).

Economically, it is important to land a horizontal well in the zone where maximum hydrocarbon production will be obtained. In the northern, onshelf portion of the study area, the Austin Chalk is fairly homogenous with fair reservoir quality and high UCS values that indicate a brittle rock. However, the section exhibits variable mineralogy and overall low source-rock quality (<0.7 wt%). Therefore, this study suggests that, in the onshelf region, there no optimal landing zone based on lithofacies distri-

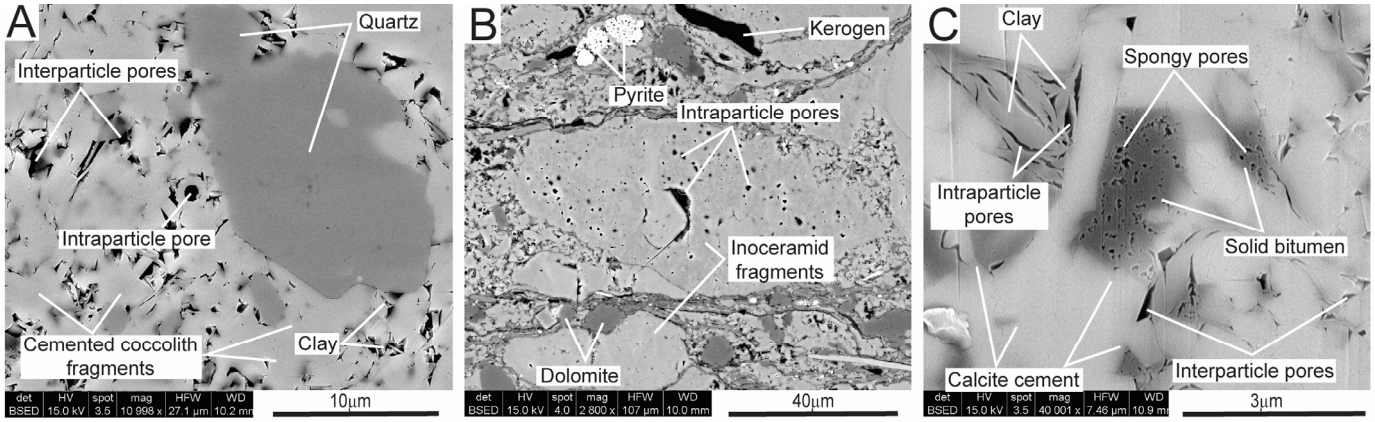

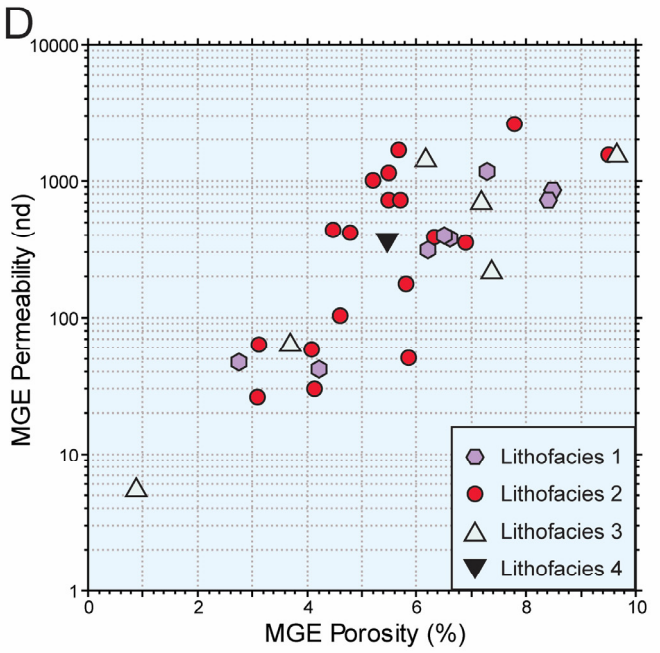

E

	Mean	Std. Dev.	Count	Minimum	Maximum	Geom. Mean
All porosity analyses (%)	5.8	2.0	34	0.9	9.6	
Lithofacies 1 porosity (%)	6.3	2.0	8	2.8	8.5	
Lithofacies 2 porosity (%)	5.6	1.7	19	3.1	9.6	
Lithofacies 3 porosity (%)	5.8	3.1	6	0.9	9.6	
Lithofacies 4 porosity (%)	5.5		1			
All perm analyses (nd)	605	628	33	6	2622	285
Lithofacies 1 perm (nd)	496	404	8	27	1188	302
Lithofacies 2 perm (nd)	647	721	18	5.6	2622	298
Lithofacies 3 perm (nd)	669	699	6	64	1555	223
Lithofacies 4 perm (nd)	344		1			344

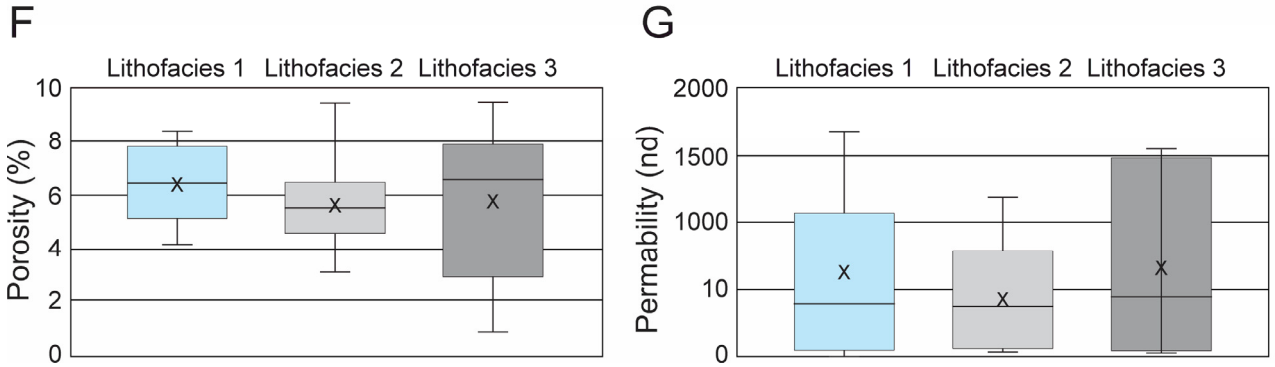

Figure 13. Pore types and reservoir quality. (A) SEM backscatter image showing coccolith hash matrix with common interparticle pores, some containing clay platelets. Minor intraparticle pores can be observed within coccolith spines. A quartz silt grain with overgrowth is also present. No. 1 McShane Trust; 14,479.3 ft (4413.3 m). (B) Intraparticle pores within inoceramid fragments as seen in a SEM backscatter image. No. 1 McShane Trust; 14,467.3 ft (4409.6 m). (C) SEM backscatter image showing organic-matter-filled spongy pores in solid bitumen. Some clay minerals between coccolith elements have intraparticle pores between platelets. Right side of the sample has interparticle pores. No. 1 McShane Trust; 14,467.3 ft (4409.6 m). (D) Plot of modified gas expansion (MGE) porosity versus MGE permeability where each datapoint is differentiated by lithofacies. (E) Descriptive statistics. (F and G) Box plot showing comparison of the different porosity and permeability by lithofacies. Box = interquartile range; horizontal line in box = median; X = mean; and vertical line = minimum to maximum range.

bution to obtain maximum production, but the entire section has the potential to be a productive reservoir across the region. In contrast, in the stratigraphic section on the upper slope, there are two potential zones for landing a horizontal well. The lower zone is similar to the updip, onshelf Austin Chalk section and has the same attributes listed for that section. The upper zone along the upper slope is more heterogeneous with burrowed and laminated cycles throughout. This zone offers better source-rock quality, which may be self-sourcing similar to unconventional shale reservoirs, but the overall mechanical strength is lower and the weaker laminated beds may impede fracture propagation.

ACKNOWLEDGMENTS

We want to recognize the State of Texas Advanced Reservoir Research (STARR) program at the Bureau of Economic Geology at the University of Texas at Austin for the major support of this investigation. Support was also received from the Carbonate Reservoir Characterization Research Laboratory (RCRL) at the Bureau of Economic Geology and associated sponsors. We appreciate the reviews of the manuscript by Tom Ewing and Lowell Waite. Meredith Faber of the Bureau of Economic Geology edited this manuscript, and we recognize and appreciate their effort. We want to recognize Michael Cervantes of Continental Resources, Travis Loseke and Laura Unverzagt of Blackstone Minerals, and Chrystianto Mardi of BP America/BXP Energy for discussion on this area of the Austin Chalk. Publication authorized by the Director, Bureau of Economic Geology, Jackson School of Geosciences, University of Texas at Austin.

REFERENCES CITED

Anderson, E. G., 1979, Basic Mesozoic study in Louisiana, the northern coastal region and the Gulf Basin Province: Louisiana Geological Survey Folio Series 3, Baton Rouge, 58 p.

Arthur, M. S., and B. Sageman, 1994, Marine black shales: Depositional mechanisms and environments of ancient deposits: Annual Review of Earth and Planetary Sciences, v. 22, p. 499–551.

Berg, R. R., and A. F. Gangi, 1999, Primary migration by oil-generating microfracturing in low-permeability source rocks—Application to the Austin Chalk, Texas: American Association of Petroleum Geologists Bulletin, v. 83, p. 727–756.

Blakey, R., 2011, Western North America series, <www.cpgeosystems.com/paleomaps.html>.

Boucot, A. J., 1990, Evolutionary paleobiology of behavior and coevolution: Elsevier Science Publishers, 724 p.

Brooks, D., X. Janson, and C. K. Zahm, 2016, The effect of sample volume on micro-rebound hammer UCS measurements in Gulf Coast Cretaceous carbonate cores: Gulf Coast Association of Geological Societies Journal, v. 5, p. 189–202.

Cooper, J .R., A. G. Godet, and M. C. Pope, 2020, Tectonic and eustatic impact on depositional features in the Upper Cretaceous Austin Chalk Group of south-central Texas, USA: Sedimentary Geology, v. 401, 17 p.

Corbett, K., M., Friedman, and J. Spang, 1987, Fracture development and mechanical stratigraphy of the Austin Chalk, Texas: American Association of Petroleum Geologists Bulletin, v. 71, p. 17–28.

Dawson, W. C., B. Katz, and V. D. Robison, 1995, Austin Chalk petroleum system, Upper Cretaceous, southeastern Texas—A case study: Gulf Coast Association of Geological Societies Transactions, v. 45, p. 157–163.

Dravis, J. J., 1981, Depositional setting and porosity evolution of the Upper Cretaceous Austin Chalk Formation, south-central Texas: South Texas Geological Society Bulletin, v. 22, p. 4–14.

Eldrett, J. S., C. Ma, S. C. Bergman, B. Lutz, J. G. Gregory, P. Dodsworth, M. Phipps, P. Hardas, D. Minisini, and A. Ozkan, 2015, An astronomically calibrated stratigraphy of the Cenomanian, Turonian and earliest Coniacian from the Cretaceous Western Interior Seaway, USA: Implications for global chronostratigraphy: Cretaceous Research, v. 56, p. 316–344.

Espitalié, J., J. L. Laporte, M. Madec, F. Marquis, P. Leplat, J. Paulet, and A. Boutefeu, 1977, *Méthode rapide de caractérisation des roches mères, de leur potentiel pétrolier et de leur degré d'évolution*: *Revue de l'Institut Français du Petrole et Annales des Combustibles Liquides*, v. 32, p. 23–43.

Ewing, T. E., 2013, Stratigraphy of the Austin, Eagle Ford, and Anacacho formations and its influence on hydrocarbon resources, Pearsall field area, South Texas: Gulf Coast Association of Geological Societies Transactions, v. 63, p. 213–225.

Ferrill, D. A., K. J. Smart, R. N. McGinnis, A. P. Morris, and K. D. H. Gulliver, 2017, Influence of structural position on fracturing in the Austin Chalk: Gulf Coast Association of Geological Societies Journal, v. 6, p. 189–200.

Grabowski, G. J., Jr., 1984, Generation and migration of hydrocarbons in the Upper Cretaceous Austin Chalk, south-central Texas, *in* J. G. Palacas, ed., Petroleum geochemistry and source rock potential of carbonate rocks: American Association of Petroleum Geologists Studies in Geology 18, Tulsa, Oklahoma, p. 97–115.

Griffith, C., M. Pope, K. Gillespie, A. Godet, and D. Minisini, 2019, Facies in the Lower Austin Chalk Group, from a roadcut on U.S. 90 and a core behind the outcrop, near Langtry, Texas: GeoGulf Transactions, v. 69, p. 79–95.

Hooks, D. J., and S. S. Hubbard, 1994, The Austin Chalk of Brookeland Field (East Texas, USA)—Importance of an integrated interdisciplinary approach in exploiting a classic fractured reservoir: European Association of Petroleum Geologists/ Association of Petroleum Geologists Special Conference on Chalk, Copenhagen, Denmark, September 7–9, 1994, p. 76–78.

Hunt, J. M., and A. P. McNichol, 1984, The Cretaceous Austin Chalk of South Texas—A petroleum source rock, *in* J. G. Palacas, ed., Petroleum geochemistry and source rock potential of carbonate rocks: American Association of Petroleum Geologists Studies in Geology 18, Tulsa, Oklahoma, p. 117–125.

Lafargue, E., F. Marquis, and D. Pillot, 1998, Rock-Eval 6 applications in hydrocarbon exploration, production and soil contamination studies: *Revue de l'Institut Francais du Petrole*, v. 53, p. 421–437.

Lock, B. E., 1984, Channels in resedimented chalks, Cretaceous Gulf Coastal Province of Texas and Mexico: Gulf Coast Association of Geological Societies Transactions, v. 34, p. 373–382.

Locklair, R. E., and B. B. Sageman, 2008, Cyclostratigraphy of the Upper Cretaceous Niobrara Formation, Western Interior, U.S.A.: A Coniacian-Santonian orbital timescale: Earth and Planetary Science Letters, v. 269, p. 540–553.

Longman, M. W., B. A. Luneau, and S. M. Landon, 1998, Nature and distribution of Niobrara lithologies in the Cretaceous western interior of the Rocky Mountain region: The Mountain Geologist, v. 35, p. 137–170.

Loucks, R. G., R. M. Reed, S. C. Ruppel, and U. Hammes, 2012, Spectrum of pore types and networks in mudrocks and a descriptive classification for matrix-related mudrock pores: American Association of Petroleum Geologists Bulletin, v. 96, p. 1071–1098.

Loucks, R. G., S. C. Ruppel, and G. Frébourg, 2013, Stop 7: Atco Chalk Member (Basal Austin Chalk Group), *in* S. C. Ruppel, R. G. Loucks, and G. Frébourg, eds. Guide to field exposures of the Eagle Ford–equivalent Boquillas Formation and related Upper Cretaceous units in southwest Texas: Bureau of Economic Geology Guidebook, Austin, Texas, p. 115–140.

Loucks, R. G., 2018, Eagle Ford–A (Boquillas–A) depositional setting and processes in southwest Texas: An example of deeper-water, below-storm-wave base carbonate sedimentation on a drowned shelf: Gulf Coast Association of Geological Societies Journal, v. 7, p. 59–78.

Loucks, R. G., J. R. Lambert, K. Patty, T. E. Larson, R. M. Reed, and C. K. Zahm, 2020a, Regional overview and significance of the mineralogy of the Upper Cretaceous Austin Chalk Group, onshore Gulf of Mexico: Gulf Coast Association of Geological Societies Journal, v. 9, p. 1–16.

Loucks, R. G., T. E. Larson, Y. Z. Zheng, C. K. Zahm, L. T. Ko, J. E. Sivil, S. Peng, S. C. Ruppel, and W. A. Ambrose, 2020b,

Geologic characterization of the type cored section for the Upper Cretaceous Austin Chalk Group in South Texas: A combination fractured and unconventional reservoir: American Association of Petroleum Geologists Bulletin, v. 104, p. 2209–2245.

Loucks, R. G., and S. Peng, 2021, Matrix reservoir quality of the Upper Cretaceous Austin Chalk Group and evaluation of reservoir-quality analysis methods; northern onshore Gulf of Mexico, U.S.A: Marine and Petroleum Geology, v. 134, 11 p.

Loucks, R. G., R. M. Reed, L. T. Ko, C. K. Zahm, and T. E. Larson, 2021a, Micropetrographic characterization of a siliciclastic-rich chalk; Upper Cretaceous Austin Chalk Group along the onshore northern Gulf of Mexico, USA: Sedimentary Geology, v. 412, 19 p..

Loucks, R. G., C. K. Zahm, T. E. Larson, L. C. Zahm, and S. Peng, 2021b, Stratal architecture, lithofacies, environmental setting, depositional processes, and associated geological characteristics of the Upper Cretaceous Austin Chalk in Louisiana: Gulf Association of Geological Societies Journal, v. 10, p. 47–75.

Loucks, R. G., and R. M. Reed, 2022, Implications for carbonate mass-wasting complexes induced by volcanism from Upper Cretaceous Austin Chalk strata in the Maverick Basin and San Marcos Arch areas of south-central Texas, USA: Sedimentary Geology, v. 432, Paper 105323.

Louisiana Mineral and Energy Board, 2018, Resurgence in Austin Chalk play: Louisiana Department of Natural Resources, Baton Rouge, <www.dnr.louisiana.gov/index.cfm/page/1442>.

Lowery, C. M., M. J. Corbett, M. Leckie, D. A. Watkins, M. Romero, and A. Pramudito, 2014, Foraminiferal and nannofossil paleoecology and paleoceanography of the Cenomanian-Turonian Eagle Ford Shale of southern Texas: Palaeogeography, Palaeoclimatology, Palaeoecology, v. 413, p. 49–65.

Pearson, K., 2012, Geologic models and evaluation of undiscovered conventional and continuous oil and gas resources—Upper Cretaceous Austin Chalk, U.S. Gulf Coast: U.S. Geological Survey Scientific Investigations Report 2012–5159, 26 p.

Peng, S., and R. G. Loucks, 2016, Permeability measurements in mudrocks using gas-expansion methods on plug and crushed-rock samples: Marine and Petroleum Geology, v. 73, p. 299–310.

Peng, S., B. Ren, and M. Meng, 2019, Quantifying the influence of fractures for more-accurate laboratory measurement of shale matrix permeability using a modified gas-expansion method: Society of Petroleum Engineering Reservoir Evaluation and Engineering, v. 24, p. 1293–1304.

Petzet, G., 1995, Texas Brookeland oil-field grows into Louisiana: Oil and Gas Journal, v. 93, p. 58–59.

Phelps, R. M., C. Kerans, R. G. Loucks, R. O. B. P. Da Gama, J. Jeremiah, and D. Hull, 2013, Oceanographic and eustatic control of carbonate platform evolution and sequence stratigraphy on the Cretaceous (Valanginian-Campanian) passive margin, northern Gulf of Mexico: Sedimentology, v. 62, p. 461–496.

Reading, H. G., and J. D. Collinson, 1996, Clastic coasts, *in* H. G. Reading, ed., Sedimentary environments: processes, facies and stratigraphy: Blackwell Science, Oxford, U.K., p. 154–131.

Rijken, P., and M. L. Cooke, 2001, Role of shale thickness on vertical connectivity of fractures: Application of crack-bridging theory to the Austin Chalk, Texas: Tectonophysics, v. 337, p. 117–133.

Scholle, P. A., 1977, Chalk diagenesis and its relationship to petroleum exploration: Oil from chalks, a modern miracle?: American Association of Petroleum Geologists Bulletin, v. 61, p. 982–1009.

Stamatedes, M., 2019, Shale and chalk plays in Louisiana: Louisiana State University/Louisiana Geological Survey Oil and Gas Symposium, Baton Rouge, 15 p.

Walker, J. D., J. W. Geissman, S. A. Bowring, and L. E. Babcock, compilers, 2013, Geologic time scale version 5.0: Geological Society of America, Boulder, Colorado, <https://www.geosociety.org/documents/gsa/timescale/timescl.pdf>.

Whidden, K. J., J. K. Pitman, O. N. Pearson, S. T. Paxton, S. A. Kinney, N. J. Gianoutsos, C. J. Schenk, H. M. Leathers-Miller, J. E. Birdwell, M. E. Brownfield, L. A. Burke, R. F. Dubiel, K. L. French, S. B. Gaswirth, S. S. Haines, P. A. Le, K. R. Marra, T. J. Mercier, M. E. Tennyson, and C. A. Woodall, 2018, Assessment of undiscovered oil and gas resources in the Eagle Ford Group and associated Cenomanian-Turonian strata, U.S. Gulf Coast, Texas, 2018: U.S. Geological Survey Fact Sheet 2018–3033, 4 p., <https://pubs.usgs.gov/fs/2018/3033/fs20183033.pdf>.

Wiltschko, D. V., K. P. Corbett, M. Friedman, and J. H. Hung, 1991, Predicting fracture connectivity and intensity within the Austin Chalk from outcrop fracture maps and scanline data: Gulf Coast Association of Geological Societies Transactions, v. 41, p. 702–718.

Zahm, C. K., and M. Enderlin, 2010, Characterization of rock strength in Cretaceous strata along the Stuart City Trend, Texas: Gulf Coast Association of Geological Societies Transactions, v. 60, p. 693–702.